

12-1-2012

Novel Production Techniques of Radioisotopes Using Electron Accelerators

Daniel Robert Lowe
University of Nevada, Las Vegas, aniqofzero@yahoo.com

Follow this and additional works at: <https://digitalscholarship.unlv.edu/thesesdissertations>



Part of the [Nuclear Commons](#), and the [Nuclear Engineering Commons](#)

Repository Citation

Lowe, Daniel Robert, "Novel Production Techniques of Radioisotopes Using Electron Accelerators" (2012). *UNLV Theses, Dissertations, Professional Papers, and Capstones*. 1749.
<https://digitalscholarship.unlv.edu/thesesdissertations/1749>

This Dissertation is protected by copyright and/or related rights. It has been brought to you by Digital Scholarship@UNLV with permission from the rights-holder(s). You are free to use this Dissertation in any way that is permitted by the copyright and related rights legislation that applies to your use. For other uses you need to obtain permission from the rights-holder(s) directly, unless additional rights are indicated by a Creative Commons license in the record and/or on the work itself.

This Dissertation has been accepted for inclusion in UNLV Theses, Dissertations, Professional Papers, and Capstones by an authorized administrator of Digital Scholarship@UNLV. For more information, please contact digitalscholarship@unlv.edu.

NOVEL PRODUCTION TECHNIQUES OF RADIOISOTOPES USING
ELECTRON ACCELERATORS

by

Daniel Robert Lowe

Bachelor of Science in Engineering
University of Nevada, Las Vegas
2005

Master of Science, Materials and Nuclear Engineering
University of Nevada, Las Vegas
2006

A dissertation submitted in partial fulfillment
of the requirements for the

Doctor of Philosophy in Mechanical Engineering

Department of Mechanical Engineering
Howard R. Hughes College of Engineering
The Graduate College

University of Nevada, Las Vegas
December 2012

Copyright by Daniel R. Lowe, 2012

All Rights Reserved



THE GRADUATE COLLEGE

We recommend the dissertation prepared under our supervision by

Daniel Lowe

entitled

Novel Production Techniques of Radioisotopes using Electrons Accelerators

be accepted in partial fulfillment of the requirements for the degree of

Doctor of Philosophy in Mechanical Engineering

Department of Mechanical Engineering

William Culbreth, Ph.D., Committee Chair

Robert Boehm Ph.D., Committee Member

Yitung Chen, Ph.D., Committee Member

Kenneth Czerwinski, Ph.D., Graduate College Representative

Tom Piechota, Ph.D., Interim Vice President for Research &
Dean of the Graduate College

December 2012

ABSTRACT

Novel Production Techniques of Radioisotopes Using Electron Accelerators

by

Daniel Robert Lowe

Dr. William Culbreth, Examination Committee Chair
Associate Professor of Engineering
University of Nevada, Las Vegas

Non-traditional radioisotope production techniques using a compact, high power linear electron accelerator have been demonstrated and characterized for the production of ^{18}F , ^{47}Sc , ^{147}Pm , and $^{99\text{m}}\text{Tc}$ from a variety of target candidates. These isotopes are used extensively in the medical field as diagnostic and therapy radioisotopes, as well as the space industry as RTG's. Primary focus was placed on $^{99\text{m}}\text{Tc}$ as it constitutes approximately 80% of all diagnostic procedures in the medical community that use radioactive tracers. It was also the prime focus due to recent events at the Chalk River nuclear reactor, which caused global shortages of this isotope a few years ago.

A Varian K15 LINAC was first used to show proof of principle in Las Vegas. Various samples were then taken to the Idaho Accelerator Center where they were activated using an electron LINAC capable of electron energies from 4 to 25 MeV at a beam power of approximately 1 kW. Production rates, cross sections, and viability studies were then performed and conducted to assess the effectiveness of the candidate target and the maximum production rate for each radioisotope.

Production rates for ^{18}F from lithium fluoride salts were shown to be ideal at 21 MeV, namely 1.7 Ci per kg of LiF salt, per kW of beam current, per 10 hour irradiation time. As the typical hospital consumption of ^{18}F is around 500 mCi per day, it is clear that a large amount of ^{18}F can be made from a small (300 gram) sample of LiF salt. However, since there is no current separation process for ^{18}F from ^{19}F , the viability of this technique is limited until a separations technique is developed. Furthermore, the calculated cross section for this reaction is in good agreement with literature, which supports the techniques for the isotopes mentioned below.

Production rates for ^{47}Sc from vanadium oxide targets were shown to be a maximum at 25 MeV with a production rate of 2 mCi per day, assuming a 2 kW beam and a 10 kg target. While this production rate would be able to support a research environment where a single patient per day would be addressed, it is unlikely that this method would produce enough material to support a large hospital.

The production of ^{147}Pm from europium oxide targets showed that due to the large spin state differences between ^{151}Eu and ^{147}Pm , a negligible amount of ^{147}Pm can be created using the (γ, α) process. The minimum detectable limit for these experiments, given this specific isotope, was 10 nCi.

The (γ, γ') reaction was studied on ^{99}Tc to determine the production rates and cross sections for this reaction. It was found that the average production rate between 12 and 25 MeV was approximately 3 uCi/(kg*kW). Given that a single patient dose of $^{99\text{m}}\text{Tc}$ is

approximately 20 mCi, we find that we need many kilograms of technetium metal. This would produce toxic levels of technetium in the patient; therefore this method is not likely viable. It was also found, however, that the (n,n') reaction may play a significant role in the activation from ground state technetium to the metastable state.

Finally, the (γ, α) reaction that will produce ^{99m}Tc from rhodium oxide targets was quantified from energies of 12 to 25 MeV. The production rate was found to be 64 and 113 mCi/(kg*kW*day) for 19 and 25 MeV, respectively. Given a 2 kW beam and a 2 kg target, we find this technique to be a feasible method to create ^{99m}Tc in a local setting using a LINAC. By using a fast separations technique, such as selective volatilization, a process in which technetium oxide is volatilized off of rhodium oxide in a carrier gas could provide a turn-key solution for entities looking to create this radioisotope on site. A cost-benefit analysis was performed and it was found that a system such as this could produce over \$1M in revenue per year given a standard hospital usage of 40 patient doses per day.

ACKNOWLEDGEMENTS

I would like to thank my advisor, Dr. William Culbreth for his support during this project. I would also like to thank my wife for her continued support during the last 4 years while I spent many weekends at school working on this project.

TABLE OF CONTENTS

ABSTRACT.....	iii
ACKNOWLEDGEMENTS.....	vi
LIST OF TABLES.....	ix
LIST OF FIGURES.....	x
CHAPTER 1 INTRODUCTION.....	1
1.1 Review of Related Literature.....	4
CHAPTER 2 THEORY.....	7
2.1 Activation and Decay.....	7
2.2 Activation from Neutrons.....	8
2.3 Activation from Photons.....	10
2.4 Accelerator Technology.....	12
2.5 Diagnostic Isotopes.....	13
2.6 RTG Isotopes.....	15
2.7 Chemical Separation Techniques.....	15
2.8 Mechanical Separation Techniques.....	17
2.9 Bremsstrahlung Production.....	19
2.10 Calculation of Cross Sections.....	20
2.11 Differential Evolution Algorithms.....	22
2.12 Financial Analysis Techniques.....	27
CHAPTER 3 EXPERIMENTAL SETUP.....	29
3.1 Accelerator Facility.....	29
3.2 Specimen Holders.....	32
3.3 Counting Laboratories.....	34
3.4 Target Material and Form.....	39
CHAPTER 4 MODELING.....	41
4.1 Steady State Production Rates.....	41
4.2 MCNPX to Predict Reaction Rates.....	43
CHAPTER 5 RESULTS.....	45
5.1 Measured Production Rates.....	45
5.2 Cross Section Based Upon Production Rates.....	51
CHAPTER 6 CONCLUSIONS.....	55
APPENDIX I SAMPLE MCNPX INPUT DECKS.....	60
APPENDIX II DIFFERENTIAL EVOLUTION PROGRAM.....	63

APPENDIX III	SAMPLE ACTIVATION DATA SHEET.....	84
APPENDIX IV	NOMENCLATURE	88
BIBLIOGRAPHY.....		89
VITA.....		90

LIST OF TABLES

Table 2.1	Radioactivity of activated rhodium targets versus energy	22
Table 2.2	Energy groups for cross section calculation	23
Table 3.1	Masses of the targets used during the irradiation	40
Table 3.2	Irradiation details for experiments at IAC	40

LIST OF FIGURES

Figure 2.1	Energy levels and spin states of ^{13}C	7
Figure 2.2	^{27}Al neutron capture cross section, (KAERI)	9
Figure 2.3	Photonuclear cross section (γ, α) for aluminum and lead	11
Figure 2.4	Example of RF resonating cavity	12
Figure 2.5	Mechanical separation nozzle.....	18
Figure 2.6	Differential evolution algorithm outline.....	24
Figure 2.7	Example values of the objective (cost) function versus iterations	27
Figure 3.1	Experimental setup at IAC	29
Figure 3.2	Experimental setup at Varian SIP.....	30
Figure 3.3	Close up of IAC experimental setup	32
Figure 3.4	Sealed (left) and unsealed (right) specimen holders.....	34
Figure 3.5	HPGe detectors at UNLV	35
Figure 3.6	Specimen holder on HPGe detector at UNLV	35
Figure 3.7	Computer and DAQ system for HPGe detector at IAC	36
Figure 3.8	HPGe detector and shielding at IAC	37
Figure 3.9	Overhead view of HPGe detector layout at IAC	37
Figure 3.10	IAC supplied efficiency calibration for HPGe detector	38
Figure 4.1	MCNPX simulated photon spectra for the IAC LINAC	44
Figure 5.1	HPGe spectrum example from LiF target, 21 MeV	46
Figure 5.2	^{18}F production rates from a LiF target.....	46
Figure 5.3	Equilibrium plot for ^{18}F from LiF targets.....	47
Figure 5.4	^{47}Sc production from vanadium targets.....	47
Figure 5.5	Equilibrium data and curve fit for ^{47}Sc from vanadium targets	48
Figure 5.6	Production rates of $^{99\text{m}}\text{Tc}$ from rhodium targets.....	49
Figure 5.7	Equilibrium data and curve fit for $^{99\text{m}}\text{Tc}$ from rhodium targets	49
Figure 5.8	$^{99\text{m}}\text{Tc}$ production rates from ground state Tc.....	50
Figure 5.9	Results from gold activation collocated with the Tc samples	51
Figure 5.10	$[\gamma, \alpha]$ Cross section for the production of $^{99\text{m}}\text{Tc}$ from ^{103}Rh	53
Figure 5.11	$[\gamma, n]$ Cross section for the production of ^{18}F from ^{19}F	53
Figure 5.12	$[\gamma, \gamma']$ Cross section for the production of $^{99\text{m}}\text{Tc}$ from ^{99}Tc	54
Figure 5.13	$[\gamma, \alpha]$ Cross section for the production of ^{47}Sc from ^{51}V	54

CHAPTER 1

INTRODUCTION

The use of radioisotopes to trace flow through the body was proposed by George Charles de Hovesy in 1913 and saw practical use in 1927 where ^{214}Bi was used as a tracer to study the velocity of blood (van der Keur, 2010). With the invention of the cyclotron accelerator in 1931 by Ernest Lawrence, it became possible to manufacture a wide range of radioisotopes for diagnostic or therapeutic use. By 1941, the first commercial cyclotron dedicated to the production of radioisotopes for medical uses was in use at Washington University in St. Louis. The Oak Ridge nuclear reactor was used to meet the increasing demand for radiochemicals during World War II and in 1946, the Atomic Energy Commission developed the Isotope Distribution Program to facilitate the production of radioisotopes to hospitals and research laboratories. Government backing of this program, as well as the high production rates of radioisotopes within nuclear reactors, caused a significant decrease in the use of accelerators, such as the cyclotron, for their production.

Modern production of isotopes for radiotherapy and diagnostics are limited to a few reactors worldwide. The short half life of many of these isotopes requires rapid chemical separation from spent fission fuel, and the time required for transportation from the reactor site to the hospital where the material is used leads to significant loss of material through radioactive decay. Accelerator production of $^{99\text{m}}\text{Tc}$ is a prime goal since this

material is used in 80% of all radiation medical procedures around the world (Kahn, 2008).

Radioisotopes are used in a wide range of modern applications, and their production is often based upon the chemical separation of material from spent fuel obtained from nuclear reactors. Radiopharmaceuticals, including isotopes of cobalt, technetium, and fluorine, are used as radioactive tracers for identification of cancerous tumors in PET scans and diagnostic scans such as SPECT imaging. These, and other isotopes, can be used to monitor blood flow through the body, and pellets of radioactive material are routinely used to destroy cancerous tissue. Other radioisotopes are used to produce decay heat that is used to generate electricity in spacecraft. Common smoke detectors use an isotope of americium to sense the presence of smoke particles in the air while radioactive cesium and californium are used to measure soil conditions through probes dropped into boreholes.

Since the usual source of these radioactive materials is spent reactor fuel, or require a reactor neutron flux is required to create the radioisotope, specialized reactors have been developed to accommodate their production. There are few of these reactor facilities and they are located in rural areas to increase safety. This results in two problems. First, radioactive material with very short half lives used in medical treatment must be chemically or mechanically separated from spent fuel, flown to urban medical facilities, and be chemically prepared for patient treatment. Second, the remote production of these radioisotopes results in a significant loss of material during preparation and transport. A

temporary shutdown of one of these specialized reactors has a significant negative impact on human health. During a recent shutdown of the National Research Universal Reactor in Canada, the world's supply of technetium used for diagnostic scans decreased by over 50% within 3 weeks of the shutdown. The shutdown lasted for 14 months, and the technetium shortage affected millions of patients throughout North America.

In the current work, an alternative technique for producing important radioisotopes is developed. Electron accelerators can produce energetic x-rays through bremsstrahlung that are capable of transmuting elements into useful radiopharmaceuticals and thermal decay power sources. The techniques for producing technetium-99m (^{99m}Tc), fluorine-18 (^{18}F), scandium-47 (^{47}Sc) and promethium-147 (^{147}Pm) developed in this project are explained, along with the experimental verification. These techniques can help address the worldwide need for these radioisotopes and provide an alternate production method using electron accelerators.

1.1 REVIEW OF RELATED LITERATURE

As early as the 1950s, scientists studied the photonuclear processes that can occur in various materials using high power linear electron accelerators. These reactions typically create daughter nuclei that are radioactive and could be detected and quantified using standard radiation detection equipment. Haslam and Skarsgard (1950) showed that the photodisintegration process, (γ, α) , of ^{87}Rb targets in the form of RbNO_3 were possible using a 100 MeV betatron accelerator. In this reaction, a gamma ray impacting the rubidium nucleus causes the nucleus to become unstable since an alpha particle was also emitted. An alpha particle is an ionized helium nucleus. The daughter nucleus of this reaction is ^{83}Br , which decays by the emission of an electron, β^- , along with associated gamma rays of various energies, and has a half life of 2.4 hours.

The 1960s and 1970s produced a large amount of information regarding cross section measurements of photonuclear and photodisintegration processes. Cross sections are used to quantify the probability that various nuclear reactions will occur, including scattering collisions and absorption. Carver (1960) first produced the integral cross section measurements for the (γ, α) reaction in ^{51}V from 0 to 32 MeV. Eight years later, Meyer, Walters and Hummel (1968) quantified the cross sections for the same reaction in ^{51}V for energies between 20 and 300 MeV. The daughter nucleus from these reactions is ^{47}Sc which decays by β^- and a 160 keV gamma ray in coincidence.

Yagi and Kondo (1976) showed that production of ^{47}Sc was most efficient using the (γ, p) reaction in an isotopically pure ^{48}Ti target. They quantified the production rates of (γ, p) , (γ, α) and $(\gamma, p+n)$ that would produce ^{47}Sc , along with a myriad of other radioisotopes such as ^{43}Sc , ^{44}Sc , ^{48}V and ^{45}Ti , to name a few.

Photoexcitation processes, such as (γ, γ') , have been measured for a variety of target materials, including ^{99}Tc . Sekine, et. Al. (1990) experimentally determined the integral cross section and production rates of ^{99m}Tc from a ^{99}Tc target using a linear accelerator with energies between 15 and 50 MeV. This paper showed a marked difference between earlier work using indium targets but did not compare the ^{99}Tc results to previous work. According to this paper, the integral cross section for the photoexcitation process in ^{99}Tc is completely flat from 15 to 50 MeV, which has a constant value of $5.5\text{E-}27 \text{ cm}^2*\text{MeV}$.

Photonuclear and photodisintegration cross sections have also been measured in materials such as fluorine and neon. Thomson and Thompson (1979) measured the (γ, n) and (γ, α) reactions that would produce ^{18}F with a linear accelerator from 14 to 30 MeV. In the same decade, Vyver, et al (1972) produced detailed measurements of the (γ, n) reaction in natural ^{19}F from 18.75 to 33 MeV using a natural CF_2 target. The data showed the mean cross section to be approximately 5 mb in that energy range.

Separation of ^{18}F from natural fluorinated targets has been investigated by Yagi and Murano (1982) who showed that rapid and high yield synthesis of carrier free ^{18}F labeled alkyl fluorides was possible. In late 2010, Majkowska-Pilip and Bilewicz studied the

feasibility of using ^{44}Sc and ^{47}Sc as radiotherapy agents as alternates to ^{177}Lu . They concluded that ^{44}Sc was a better radiotherapy and imaging radionuclide than the traditional ^{68}Ga , while ^{47}Sc had better chemical and nuclear properties over the traditional ^{177}Lu therapy techniques.

CHAPTER 2

THEORY

2.1 ACTIVATION AND DECAY

There are approximately 255 stable isotopes that have been found in nature while there are approximately 3000 known unstable isotopes, called radioisotopes. These radioisotopes can decay by a variety of processes, including beta decay, alpha decay, internal conversion, double beta decay, positron decay and neutron decay, to name a few. The decay process of an atom is fundamentally due to the excess energy found within the unstable atom.

All atoms have a specific combination of spin states that the nucleus can fill. Radioactive decay is a result of the nucleus going from a higher energy state to a lower one. Figure 2.1 shows the 4 spin states for stable ^{13}C along with the energy band of each spin state. Here we see that the $1/2^-$ spin configuration is the ground state for this atom while $1/2^+$, $3/2^-$ and $5/2^+$ are excited states that result in a 3.089, 3.684 and 3.853 MeV energy release when this process occurs.

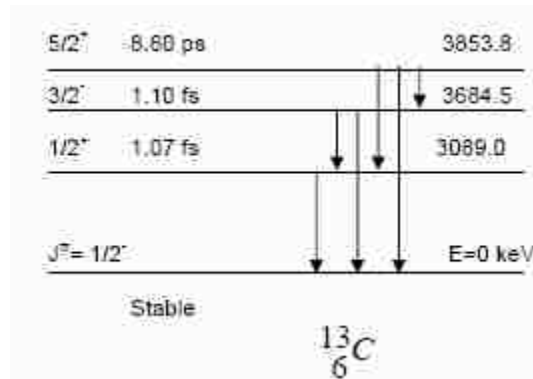


Figure 2.1 Energy levels and spin states of ^{13}C

2.2 ACTIVATION FROM NEUTRONS

Activation from neutron capture is a process where the atom captures an incoming neutron of a certain energy and raises the energy level of the nucleus. Depending on the number of protons and neutrons in said nucleus, the atom will eventually decay back down to its ground state. The process may take as little as femtoseconds or may take as long as many billions of years.

The probability for an atom to capture a neutron is called the neutron cross section. The neutron cross section is typically plotted with energy as the ordinate and the probability of the interaction occurring on the abscissa. The energy units are typically in eV or MeV, and the interaction probability unit is typically the barn, or 10^{-24} cm². One barn is roughly equivalent to the cross-sectional area of an atomic nucleus, the typical target area for a nuclear interaction with an incident particle or gamma ray. An example of a neutron capture cross section for ²⁷Al is shown in Figure 2.2.

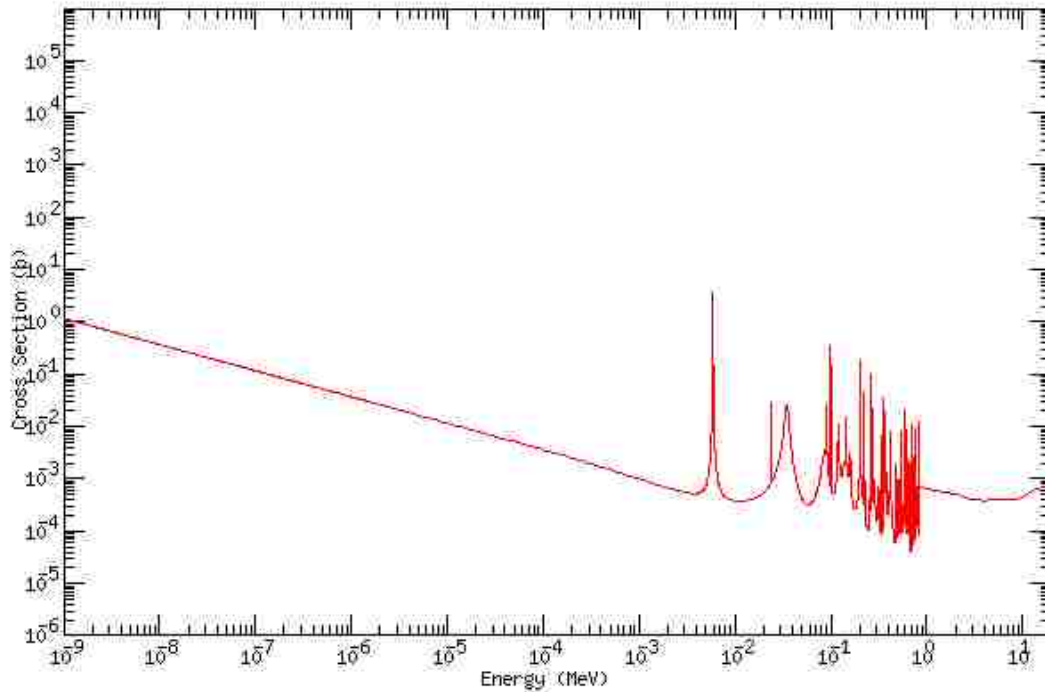


Figure 2.2 ^{27}Al neutron capture cross section, (KAERI)

When aluminum is bombarded with neutrons, the nucleus will sometimes capture the incident neutron according to the neutron cross section. If this reaction does take place, according to the equation below, a new isotope will be created, namely ^{28}Al in this case.



(2.1)

The new isotope, ^{28}Al , has a half life of 2.24 minutes and is a β - emitter. The endpoint beta energy from this decay is 2.8629 MeV and has a 1.778 MeV photon that is simultaneously emitted from this decay. As it is difficult to quantify the amount of beta particles coming from a target material, most researchers prefer to characterize the amount of a radioisotope within a sample by using the emitted photons. Detection of keV

to low MeV photons is relatively easy today with the aid of high purity germanium detectors (HPGe), which will be discussed further in the paper.

2.3 ACTIVATION FROM PHOTONS

The neutron capture cross section for all materials is continuous over most neutron energies that are studied in the laboratory system. This stems from the fact that neutron capture has a positive Q value associated with it, which means that a neutron of any energy has a nonzero probability of interaction with the nucleus over all neutron energies. Q represents the amount of mass converted into energy during a collision between a particle and a nucleus based on Einstein's famous equation, $E = m c^2$. The cross section that describes the collision between a photon and a nucleus is not continuous since the Q value for all of these reactions is negative; i.e. there is a threshold where the photon activation reactions start to take place. The following equation shows the reaction of a high energy photon incident on fluorine atom, which, in this case, causes a neutron to be emitted.



Since the Q value for this reaction is -10.432 MeV, this implies that the incident photon must have more than 10.432 MeV of energy for this reaction to take place. This exact reaction, a photon in with a neutron out, can be simply designated by (γ,n) . Reactions

involving an incident photon and an ejected particle (neutron, proton, deuteron, triton, alpha nucleus, etc) are called photonuclear events.

Photonuclear events also have cross sections associated with certain types of reactions. An example of the photonuclear cross section (γ, α) for ^{27}Al and ^{208}Pb is shown below in Figure 2.3.

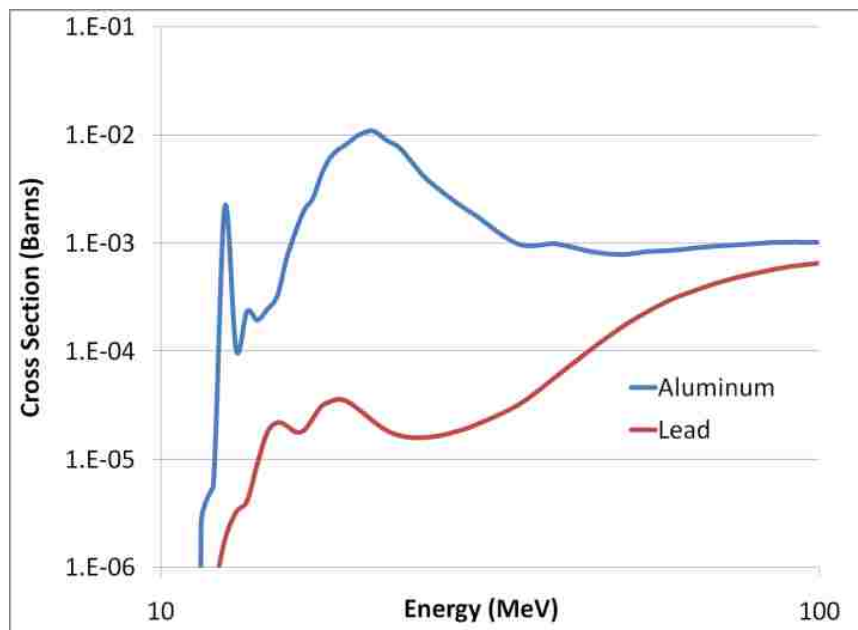


Figure 2.3 – Photonuclear cross section (γ, α) for aluminum and lead

Here we can see that threshold for the (γ, α) reaction in aluminum is slightly lower than that of lead.

2.4 ACCELERATOR TECHNOLOGY

Linear electron accelerators are composed of a variety of components with the major items being the klystron, the waveguide assembly and resonating cavity, the target and cooling systems as well as the beam focusing equipment, which is typically in the form of a quadrupole. The klystron is a device that creates high power RF from accelerating bunches of electrons through various chambers within the klystron. The main purpose of the klystron is to amplify the RF that will be used to accelerate the electrons in the resonating cavity. The waveguide assembly and resonating cavity use the high power RF created by the klystron to accelerate electrons to very high electric potentials. A cutaway of an RF resonating cavity is shown in Figure 2.4.

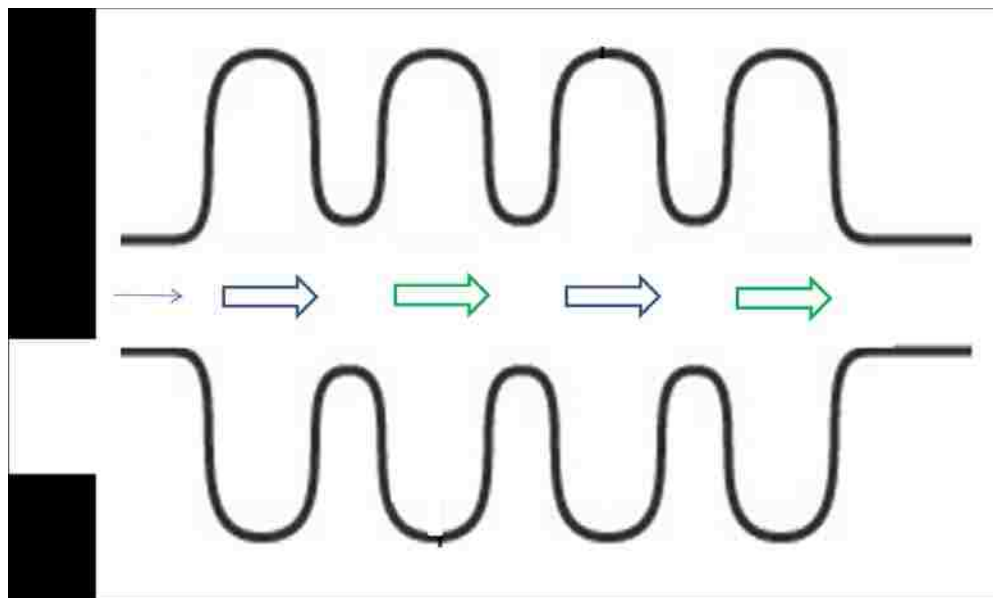


Figure 2.4. Example of RF resonating cavity

After the electrons have been accelerated through the RF cavity, they emerge at a much larger potential than when they entered. It is common for 10 keV electrons to be accelerated to 20 MeV within a few meters, typically one meter to reach a 20 MeV potential. The high energy electrons are then bombarded onto a medium to high Z, high density target to create bremsstrahlung photons, which are then used for imaging, therapy or other radiological uses.

2.5 DIAGNOSTIC ISOTOPES

Diagnostic isotopes are those used to image the human body. The image may be created from the emission of a single photon or from double 511 keV photons, called single photon emission computed tomography (SPECT) and positron emission tomography (PET), respectively. SPECT imaging processes typically use the 140 keV photon that is released when ^{99m}Tc decays to ^{99}Tc . The technetium isotope is combined with a variety of chemical compounds, such as phosphonates, bisphosphonates and tetrofosmin, to create bone scans, myocardial perfusion scans and brain scans. Other single photon emitters, such as ^{111}In , are used to scan the white blood cells in the body.

The radioisotope used for SPECT type procedures requires a few key characteristics in order for that radioisotope to be a potential candidate for use. The most important of these aspects is that the decay of the photon from the radioactive nucleus needs to be around 140 keV, plus or minus 20 keV. This criteria is driven by the fact that the detectors on SPECT imagers are optimized for the 140 keV line from ^{99m}Tc . If the new radioisotope has a decay photon of much larger or much smaller energy than 140 keV, the detector

panels may not work. The second most important aspect for the radioisotope to have is a half life that is between 60 minutes and 600 minutes. If any shorter, the logistics of transporting short lived isotopes becomes a major issue; if too long, the specific activity of the radioisotope will be too low, leading to long scan times.

PET imaging is generally always done with radioactive flourodeoxyglucose (FDG). The natural ^{19}F that is normally found in the molecule is replaced with radioactive ^{18}F . The current production method employed throughout the world is the $^{18}\text{O}(p,n)^{18}\text{F}$ reaction; 4 MeV protons are bombarded on an ^{18}O enriched water sample where the ^{18}F is later extracted and combined with the sugar molecule. Since ^{18}F is a positron emitter, there are two coincident 511 keV photons that are emitted during the decay of the nucleus. These two photons are detected by a pair of panel detectors that then calculate where the decay nucleus is in space. Over time, an image can be formed showing the relative concentrations of FDG in the body, which typically indicated a cancer site.

Characteristics of potential PET radioisotopes will be more restrictive than SPECT radioisotopes in that the PET radioisotope must be a positron emitter to work with the current detection system on PET devices. The second criteria is similar to that of a SPECT system in that the isotope must have a half life between 60 and 600 minutes for reasons discussed above. These two criteria severely limit the amount of potential candidates for PET imaging systems.

2.6 RTG ISOTOPES

Radioisotope thermoelectric generators (RTGs) are electrical power devices that derive their power from harnessing the decay heat from radioactive decay. Ideal RTG isotopes have decay modes with 100% charged particle emission; this ensures that all of the decay energy is captured locally in the device. This is why pure alpha emitters are the most common of the RTG isotopes, such as ^{238}Pu , ^{242}Cm and ^{244}Cm .

2.7 CHEMICAL SEPERATION TECHNIQUES

Chemical separation of species A from species B is, in general, a unique process that is particular to parent and daughter species. There are a variety of possible types of chemical based extraction techniques that could be applied to the irradiated targets in order to separate the desired isotope from the target material, namely solvent extraction, resin columns and/or selective volatilization.

Solvent extraction is a process that relies on the mixing of aqueous and organic phases to selectively extract a metal from a compound solution. This process relies on the forced interaction between two immiscible solutions that transfers the metal from one solution to another. This multistep process starts with the dissolved metal in an aqueous form and is contacted with an organic solution which contains an extractant that selectively attaches to the desired metal. This organic phase is then contacted with a fresh batch of aqueous solution, typically lower in acid concentration than the first step, which back extracts the desired metal. The desired metal is now in a pure aqueous form, which is a useable form

of the metal. From here, the metal could be separated by other wet chemistry techniques or by simply allowing the solution to evaporate, leaving behind the metal.

Resin columns are vertical columns that contain solid organic material called resin beads. These beads are an extractant that is typically sorbed onto an inert backbone and then placed into the column. An aqueous phase solution that contains the metal of interest, along with other constituents, is passed through the column. As the solution passes through the column, the metals separate based on their affinity to the resin beads. Those that have higher affinity travel slower through the column; those with lower affinity travel faster. The metal concentration exiting the fluid is therefore a function of flow rate, which can be optimized to select the metal of interest. This higher concentrated solution is in a more useful form in order to extract the metal from the carrier solution.

Selective volatilization separation techniques rely on the differences in volatilization temperature of solids to selectively isolate the species of interest. An example would be a mixture of three solids, A, B and C, whose volatilization points are 500 °C, 750 °C and 1000 °C, respectively. If this mixture were heated to 550 °C, only metal A would become volatilized and could be transferred from the mixture to another location by using a heated carrier gas. This method holds promise over the other techniques listed above as this is the only method where the target is not continually destroyed and reformed.

2.8 MECHANICAL SEPERATION TECHNIQUES

There are three major types of mechanical separation techniques that are used to selectively isolate heavier or lighter isotopes within a mixture. Diffusion processes, typically used to separate ^{235}U from ^{238}U , rely on the fact that the ^{235}U molecule is slightly smaller than that of the ^{238}U molecule. This allows engineers to construct specialized filters that allow only the ^{235}U molecule to pass through the membrane. Diffusion processes are the most common method in the United States to enrich uranium for power and weapons programs.

Centrifuge systems rely on small, high speed rotational turbines to spin gaseous UF_6 at high rates within tall columns that are connected in series. The heavier UF_6 (^{238}U) is spun to the outer most portions of the cylinder; the lighter UF_6 (^{235}U) is then found on the inner portion of the cylinder. This process is repeated thousands of times in order to separate the ^{235}U from the ^{238}U .

Mechanical nozzle separation was used in the 1950s as an experimental form of separating ^{238}U from ^{235}U . This nozzle, shown in Figure 2.5, is similar to the centrifuge system in that it relies on the concept that the $^{238}\text{U F}_6$ molecule is slightly heavier than the $^{235}\text{U F}_6$ molecule. This nozzle uses a hydrogen feed gas that transports the UF_6 gas through the nozzle at high speeds; the light and heavy fractions of UF_6 are then separated by a wedge piece.

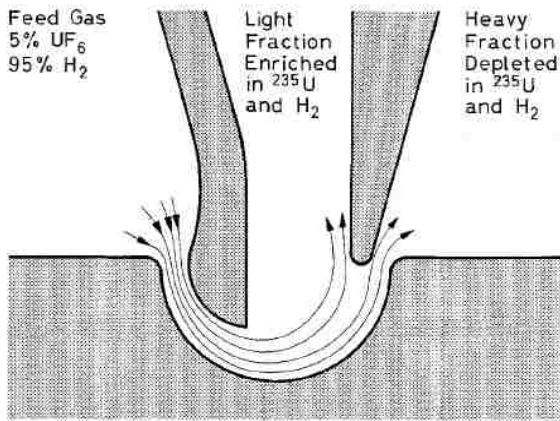


Figure 2.5 Mechanical separation nozzle

The latest technology to emerge in the isotopic separations field is selective laser ablation. This technique relies on the scientific principle that a finely tuned laser can be applied to a surface that is coated with ²³⁸U and ²³⁵U; the laser is tuned such that only the ²³⁵U atom is liberated from the surface. This is possible because the resonant absorption of light is isotope specific.

All four separation processes listed above require large infrastructure and also have large power consumption requirements for operation. For this reason, only enrichment of uranium isotopes is typically done in this fashion, and only the government is large enough to fund and operate these types of plants. A typical diffusion enrichment facility can occupy over 100 acres of land and consume up to 50 MW of power. For the above reasons, the three/four isotopic separation techniques are not likely candidates for separating diagnostically useful isotopes from their targets; a new, more efficient method will have to be developed for the medical community.

2.9 BREMSSTRAHLUNG PRODUCTION

The photons that are used to create the photoactivation processes described above are a result of the bremsstrahlung process. The photons are created when they interact with an atom of nearby material, causing the electron to change direction and velocity. This change in energy produces photons, namely bremsstrahlung photons, or “breaking” photons. While the process is completely random, an empirical expression was formed by G. Castellano, et. al., shown below for electron end point energies less than 20 keV.

$$I = \alpha \cdot i \cdot t \cdot g(Z, E_o, E) \quad (2.3)$$

Where α is a geometric detection factor, i is the beam current, t is the live time and

$$g(Z, E_o, E) = \sqrt{Z} \frac{E_o - E}{E} \left(-54.86 - 1.072E + 0.2835E_o + 30.4 \ln Z + \frac{875}{Z^2 E_o^{0.08}} \right) \quad (2.4)$$

Castellano, et. al., showed that the above equation was not properly matched to the experimental results and showed that a more accurate estimate, which was beam current and live time independent, was the following:

$$g(Z, E_o, E) = \sqrt{Z} \frac{E_o - E}{E} \left(-73.90 - 1.2446E + 36.502 \ln Z + \frac{148.5E_o^{0.1293}}{Z} \right) * \\ [1 + (-0.006624 + 0.0002906E_o) \frac{Z}{E}] \quad (2.5)$$

The equation above represents the empirical formula for the bremsstrahlung x-rays produced from electrons bombarding a target of material Z with electron end point energy of E_0 .

2.10 CALCULATION OF CROSS SECTIONS

Measurement of the (γ , α) cross section for the production of ^{99m}Tc from ^{103}Rh targets, for example, is complicated if a bremsstrahlung source is used since the gamma ray energy is spread across the entire energy range from zero to the maximum energy of the accelerator electrons. The quantity of activated product in a bremsstrahlung target is based upon the integral of the product of cross section and gamma ray flux. The reaction rate that produces ^{99m}Tc may be represented by:

$$\frac{dR}{dt} = \int_{E=0}^{E_{max}} \phi_{\gamma}(E) \sigma_{\gamma,\alpha}(E) dE \quad (2.6)$$

This equation demonstrates that experiments conducted with the same target material require knowledge of the cross section, $\sigma_{\gamma,\alpha}(E)$ as a function of gamma ray flux, $\phi_{\gamma}(E)$. In these experiments, we want to compute the cross-section as a function of gamma energy based upon a limited number of experiments. For the measurement of ^{99m}Tc production from rhodium, seven experiments were conducted where the radioactivity of the target was measured for seven different accelerator energies, E_{max} . Given values of the cross section, the radioactivity of ^{99m}Tc was calculated from the equation:

$$\alpha_{Tc99m}(E) = \frac{\lambda_2 \lambda_{1T} N_{10}}{\lambda_{1T} - \lambda_{2T}} (e^{-\lambda_{2T}t} - e^{-\lambda_{1T}t}) e^{-\lambda_{2T}t_R} \quad (2.7)$$

Where,

$$\lambda_{1T} = \int_{E=0}^{E_{max}} \varphi_{\gamma}(E) \sigma_{\gamma\alpha}(E) dE$$

$$\lambda_2 = \ln(2) / \left(\frac{t_1}{2} \right)_{Tc-99m} \quad \text{This is the decay constant for } ^{99m}\text{Tc}.$$

$$\lambda_{2T} = \lambda_2, \text{ in the absence of gamma interaction with } ^{99m}\text{Tc}.$$

$$N_{10} = \text{initial number of } ^{103}\text{Rh atoms in the target}.$$

To calculate the cross section, an optimization technique was used to minimize the error between the measured radioactivity of the ^{99m}Tc sample in each experiment versus the value calculated by Equation 2.6. The optimization technique minimizes the objective function defined as the standard deviation between measured and computed radioactivity as a function of the peak x-ray energy, $E_{i-\max}$, in each measurement. For “N” experiments,

$$f(\sigma_{\gamma,\alpha}(E)) = \sqrt{\frac{\sum_{i=1}^N (\alpha_{measured} - \alpha_{computed})^2}{N-1}} \quad (2.8)$$

This objective function is minimized if the ideal cross section distribution, $\sigma_{\gamma,\alpha}(E)$, is determined. Since the objective function, F , is not differentiable and is nonlinear, optimization routines based upon differentiation and Newton’s method are not well suited to find the optimal cross section distribution, $\sigma_{\gamma,\alpha}(E)$. There are several methods that do work well with this kind of problem, including the Simplex Method and Nelder-Mead algorithm. For this work, a relatively new technique called differential evolution (DE)

was used to find the optimal cross section for sets of experiments. The method converges relatively quickly and worked well.

2.11 DIFFERENTIAL EVOLUTION ALGORITHMS

Differential evolution (DE) was developed by Storn and Price in 1996 as a method of finding an optimal solution to problems that have objective functions that cannot be differentiated, are multidimensional, or are nonlinear. This technique is based upon an evolutionary algorithm that mutates sets of solutions to find the solution that best optimizes the objective function. A vector of possible solutions is constantly recombined and mutated to seek the best possible solution. The DE technique can work with multidimensional problems that are difficult to solve with other optimization methods. For the ^{99m}Tc experiments, the production rate of the radioisotope was measured for seven different accelerator voltages as shown in Table 2.1.

Index	Accelerator	Radioactivity
	Maximum	of Tc-99m
	Electron	
	Energy	
	(MV)	(μCi)

Table 2.1 Radioactivity of activated rhodium targets versus energy

In this case, the cross sections were organized into a vector of seven values, X_j , for $j = 0$ to 6, representing the “elements” of the energy spectrum shown in Table 2.2.

Cross Section	Energy
Index	Range
	(MeV)
[Redacted content]	

Table 2.2 Energy groups for cross section calculation

“D” represents the number of elements needed to solve the objective function, $f(X)$. The optimal solution vector was then determined using the evolutionary algorithm outlined in Figure 2.6.

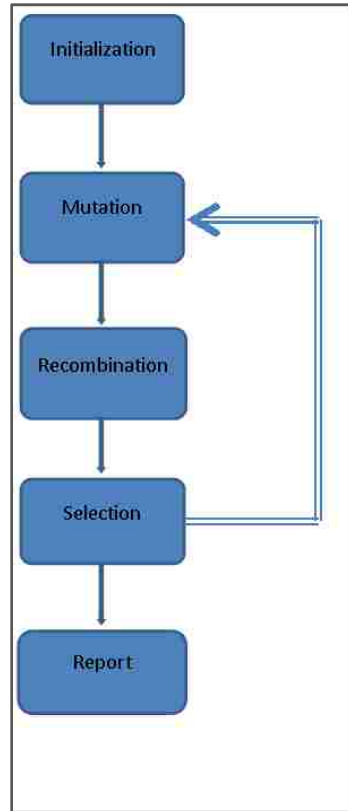


Figure 2.6 Differential evolution algorithm outline

In the differential evolution (DE) algorithm, a population of “N” of possible solution vectors is formed with an index “j”. These “N” vectors within the population are mutated and recombined to determine a new generation, “G,” of possible optimal vector solutions. The nomenclature used to describe each generation of the population is x_i^G where $i = 0 \rightarrow N$ vectors in the population. The symbol x_i^G refers to all elements in vector “i.” The individual elements of each solution vector are referenced by the index “j” as in $x_{j,i}^G$ for $j = 0 \rightarrow D$.

The population of solution vectors is initialized by randomly selecting element values for the “N” vectors in the population. The values that each element can be filled with are

limited by the upper and lower bounds allowable for these parameters. For example, in cross section analysis, all elements must contain positive, real values since cross sections cannot be negative or imaginary.

Each of the “N” vectors in the population is mutated using a random selection of parameters, recombined with other vectors, and selected to mutate other vectors. Mutation helps to expand the search space of possible parameters. Recombination is used to identify vectors that best minimize the objective function, $F(x)$. Now, for each vector, x_i^G , randomly choose three vectors from the population to be labeled: x_{r1}^G , x_{r2}^G , and x_{r3}^G . The indices I , $r1$, $r2$, and $r3$ must be distinct with no duplications. Next, form a new “donor” vector, v_i^G by using the weighted difference of the selected vectors:

$$v_i^{G+1} = x_{r1}^G + F * (x_{r2}^G + x_{r3}^G) \quad (2.9)$$

Where, $0 \leq F \leq 2$. The donor vector is used to form new possible solution vectors by recombining vectors from the previous generation.

Next, successful solution vectors from the previous generation, G , are recombined into the new generation population, $G + 1$. Elements in the donor vector, v_i^{G+1} , are combined with elements of each vector from the previous generation with a probability of “CR.”

These are used to form a trial vector, u_i^{G+1} as shown in the scheme below.

$I_{random} = \text{random integer from } 0 \text{ to } D$
If ($rnd \leq CR$) or ($j = I_{random}$) then

$$u_i^{G+1} = v_i^{G+1}$$

else if ($rnd > CR$) *and* ($j \neq I_{random}$) *then*

$$u_i^{G+1} = x_i^G$$

end if

Each target vector, x_i^G , is compared with the trial vector, v_i^{G+1} , to find out which one best minimizes the objective function, $f(x)$. The scheme used to assign x_i^{G+1} to the new population is shown below.

For $i=1$ *to* N

If $f(u_i^{G+1}) \leq f(x_i^G)$ *then*

$$x_i^{G+1} = u_i^{G+1}$$

else

$$x_i^{G+1} = x_i^G$$

end if

next i

Mutation, recombination, and selection are repeated until some criterion is reached.

Possible criterion include: the maximum number of generations to be considered has been reached; the maximum allowable computational time, or wall clock time, has been reached; the objective function has converged on some value and is not changing; and the objective function, or “cost,” has decreased below a desired tolerance.

The objective function for over 840 generations of solutions is shown in Figure 2.7 for a problem based on the optimal selection of cross sections for ^{99m}Tc production from ^{103}Rh . The convergence rate shown in the figure is typical for an evolutionary algorithm where

random generation of solution vectors will occasionally lead to an increase in the average objective function or cost function for the population of “N” vectors. These perturbations recede as the number of iterations increases. In general, the DE technique converges rapidly for a wide range of problems.

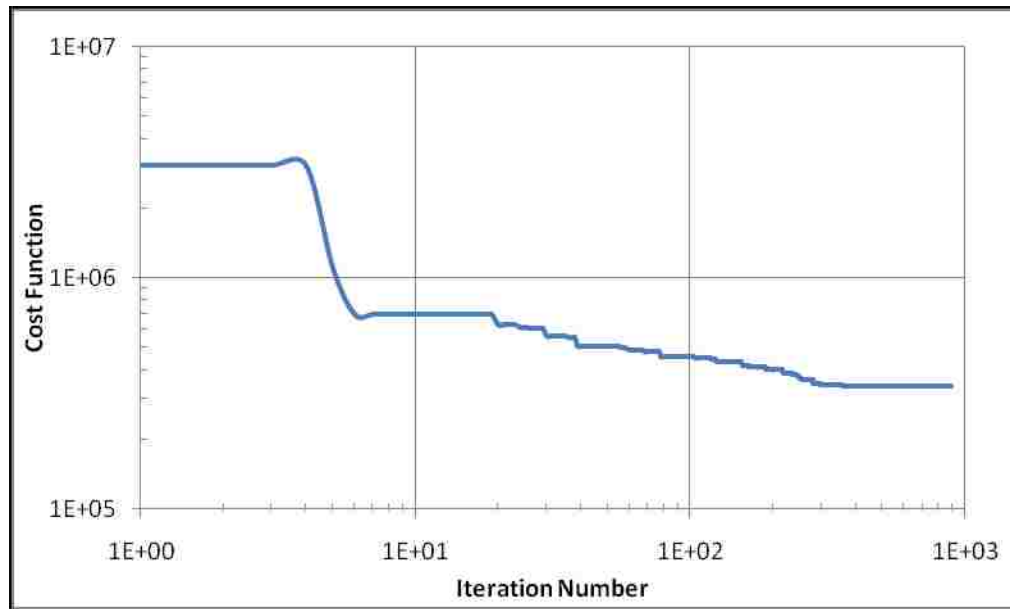


Figure 2.7 Example values of the objective (cost) function versus iterations

2.12 FINANCIAL ANALYSIS TECHNIQUES

There are a myriad of financial analysis techniques that can be applied to a system to gauge the monetary aspects of a given technology relative to current technologies. The two most common types of analyses that are performed are Cost-Benefit Analyses (CBA) which determine if the investment is sound and a Return on Investment (ROI) calculation which gives a more detailed assessment on the potential profit earnings for the said technology.

A Cost-Benefit Analysis is useful to assess the appropriateness of one technology compared to another. A CBA typically has an 8 to 10 step process in order to determine this. The steps generally consist of the following: find alternative projects/programs/technologies, assess the current technology and major players in the market, compile cost/profit estimates for new technology, predict costs and profits for life of the system, convert costs/profits into net present worth dollars, apply reductions in cost (i.e. tax benefits, etc.), complete a sensitivity analysis and finally compile all data. The summary of this type of technique will shed light on the overall prospects of the new technology relative to current processes.

If the CBA conclusion is that the new technology is appropriate and profitable, an ROI may be performed in order to provide more detail on the profit potential for the system or process. An ROI differs from a CBA in that an ROI is more specific to estimating the profit of a system whereas the CBA is a more general overview of a system. An ROI is generally defined as the following:

$$\text{ROI} = (\text{Gain of Investment} - \text{Cost of Investment}) / \text{Cost of Investment} \quad (2.10)$$

When evaluating a new system with an ROI calculation, we would expect that a profitable system will have an ROI greater than 1.

CHAPTER 3

EXPERIMENTAL SETUP

3.1 ACCELERATOR FACILITY

There were two irradiation facilities that were used to activate the specimens for this project. The Varian K15 electron accelerator was used at the Las Vegas location in the Varian Security and Inspections Products irradiation cells while a 25 MeV electron accelerator was used at the Idaho Accelerator Center (IAC) for the majority of the activation and cross section measurements. The majority of the work was done at IAC for two reasons: the IAC LINAC is capable of higher end point energies and is easily tunable whereas with the Varian K15 it is more difficult to tune and verify the end point energy of the electrons.



Figure 3.1. Experimental setup at IAC

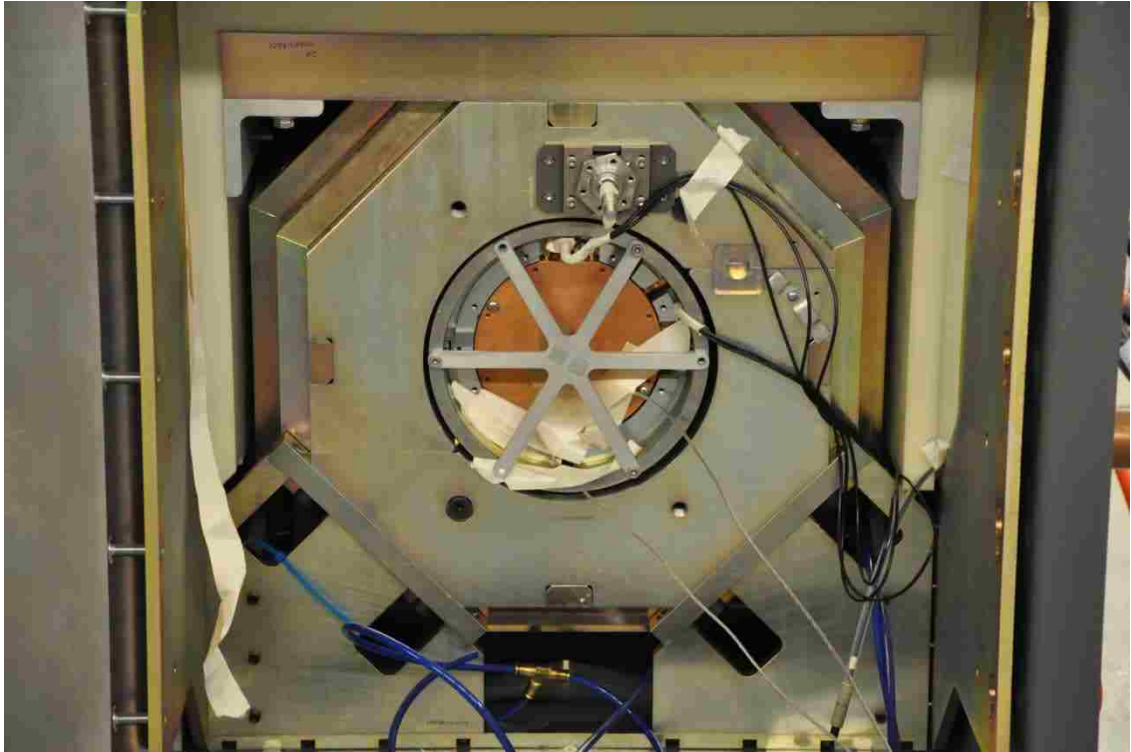


Figure 3.2 Experimental setup at Varian SIP

The Varian K15 unit is a high current electron accelerator that has a nominal end point energy of 15 MeV. It is powered with a 5 MW Klystron and is capable of delivering up to 100 micro amps DC equivalent of beam current. The bremsstrahlung converter is composed of a copper and tungsten composite and is cooled with a water jacket. The output photon dose rate of the machine is 150 Gy/min at 1 meter (equivalent to 2000 Gy/min at the bremsstrahlung converter). The unit is somewhat compact, measuring only 5 feet wide, 10 feet long and 5 feet tall. A picture of the K15 unit that was used is shown in Figure 3.2.

The IAC 25 MeV accelerator is a 1960s era machine that was retrofitted after it came to the IAC. It was originally used in a therapy machine (details of which brand were not disclosed) and was taken apart, separated, retuned and placed into a research

configuration that has multiple beam lines, steering magnets, focusing magnets, etc. The machine is easily tuned from 25 MeV to about 13 MeV and then from 11 MeV to about 4 MeV. The gap between 11 and 13 MeV is due to the fact that the energy switch must be changed at 12 MeV and the machine does not function well near this 12 MeV setting.

The experimental setup at IAC is shown below in Figure 3.3. The electron beam is sent through the focusing magnets on the left of the image, sent through a small vacuum tube where they pass through a very small vacuum window (0.001" aluminum window) and ultimately collide with the water cooled bremsstrahlung converter, seen in Figure 3.3 with the hoses coming towards the reader. A secondary aluminum water block was necessary, according to the IAC staff, due to electrons that make it past the bremsstrahlung converter. These extraneous electrons have been known to heat up small samples and catch fire. Therefore, an additional electron block was added. The specimen holder was placed 5 inches from the bremsstrahlung converter and was composed of tape spanning two bars.

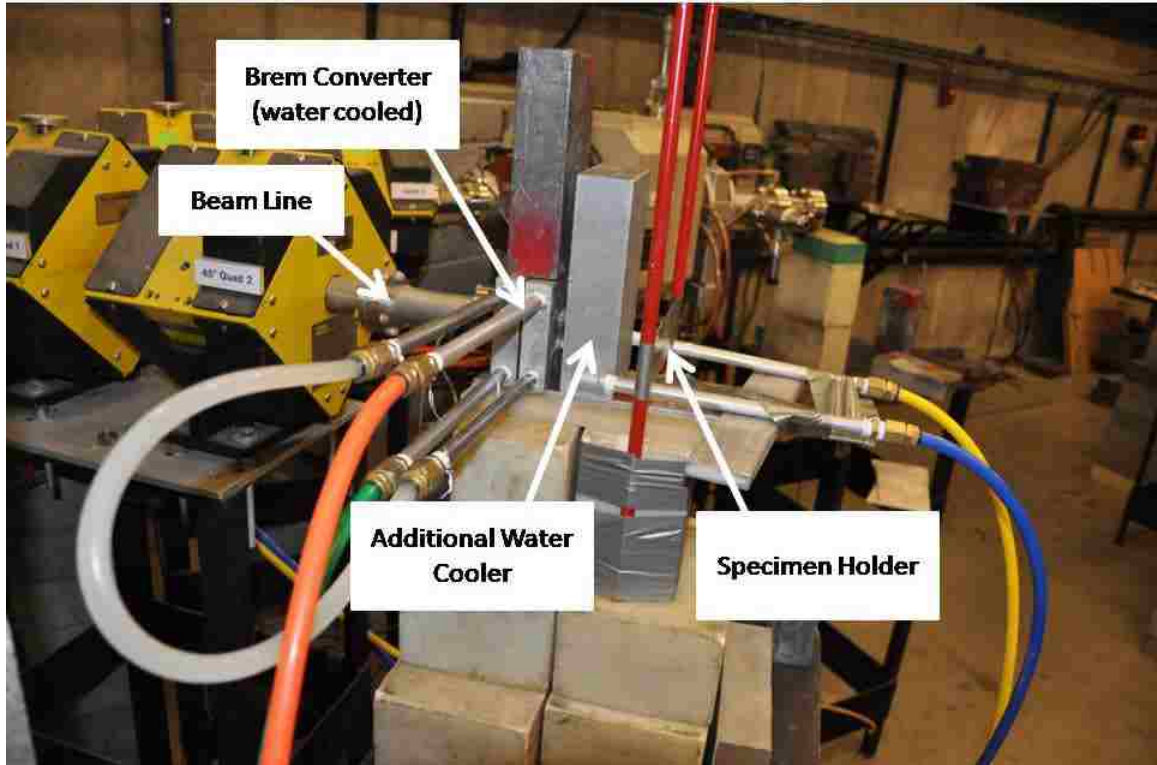


Figure 3.3 Close up of IAC experimental setup

In order to ensure the electron beam was centered on the exit flange, small plates of glass were exposed to the electron beam before each irradiation. This exposure leaves a small burned spot on the glass, showing the user where the electron beam is centered and how wide the electron beam is. A laser system was then placed in the lab to mark the position of the electron beam. Finally, the samples were placed on the tape holders where the laser dot was positioned to ensure correct position for each irradiation.

3.2 SPECIMEN HOLDERS

A significant effort was placed into the material selection and fabrication of the specimen holders for these experiments. There are many criteria that had to be satisfied in order to ensure high quality from the HPGe data. The sample holder material should contain only

one natural isotope, should have good malleability and workability, should have a daughter product from (γ , n) that has a very short half life (most (γ , n) reactions produce a positron emitter which would be indistinguishable from the ^{18}F emitter unless the half life is less than a few minutes, in which case all of the daughters will have decayed away before counting of the ^{18}F took place) and finally have a neutron capture product whose gamma lines do not coincide with any gamma lines of interest from any of the studied target materials.

Off-the-shelf aluminum would seem to be a good candidate for the sample holder as it satisfies most requirements above. 6061 aluminum was first tried as a baseline case and was shown to have many unwanted activation products. This is due to the fact that most alloyed aluminums have between 3% and 6% of impurities such as silicon, iron, copper, manganese, magnesium, chromium, zinc and others. The solution to this problem was to use 5N pure aluminum (99.999%). Activation of this material was shown to have essentially zero detectable activation due to ^{26}Al having a long half life, making the activity of ^{26}Al low, and due to ^{28}Al having such a short half life of 2.24 minutes, so that it decays away before the sample holder can be counted on the HPGe. Therefore all of the specimen holders that were used in this experiment were fabricated from 5N aluminum, as shown in Figure 3.4.



Figure 3.4 Sealed (left) and unsealed (right) specimen holders

Special attention was also given to the placement of the sample relative to the wall of the holder as well as the way the system was sealed. The specimen needed to have as little aluminum between it and the detector as possible as the aluminum would attenuate the signal, leading to large sources of error. In order to combat this, the specimen hole was drilled such that the minimum amount of aluminum material between the sample and the detector was 0.010 in. To minimize the risk of using an unsealed radioactive source, the target materials were sealed by pressing a 5N aluminum pin into the hole drilled in the specimen body. By using a press fit, the samples become permanently sealed, reducing, if not eliminating, the possibility of contamination from an unsealed radioactive source.

3.3 COUNTING LABORATORIES

Since there were two experimental facilities, two counting labs were necessary to identify and quantify the amount of radioactive material produced in the accelerators. At UNLV,

the HPGe counting lab houses 10 HPGe detectors, of which two were used for this experiment, as shown in Figure 3.5. Figure 3.6 shows the activated specimen holder/target material being placed above the HPGe detector at a measured height. The detectors are calibrated to these heights and can therefore be used to quantify the source strength of the sample being counted.



Figure 3.5 HPGe detectors at UNLV

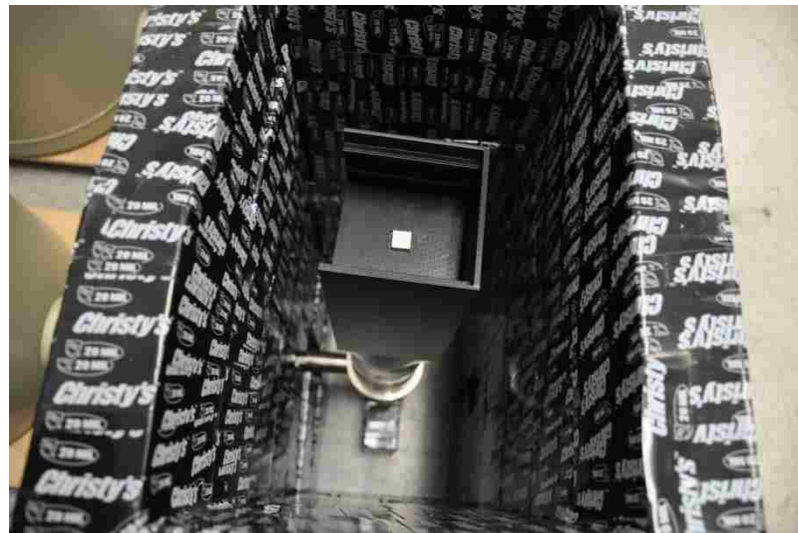


Figure 3.6 Specimen holder on HPGe detector at UNLV

The counting laboratory at IAC is similar to the one at UNLV but houses only two detectors, one of which was not operational. The HPGe detector system that was used at IAC is shown in Figures 3.7 and 3.8. A traditional NIM-bin style pre amplifier, spectroscopy amplifier and MCA were used in conjunction with a Canberra coaxial HPGe crystal.



Figure 3.7 Computer and DAQ system for HPGe detector at IAC

The detector system has preconfigured counting locations as shown in Figure 3.9. The multiple positions are necessary in order to accommodate a large range of source strengths from activated samples. The weaker sources would be placed closer to the detector for added efficiency while the stronger sources need to be placed further away

from the detector; if a strong source is placed close to the detector, the dead time of the detector is generally high and therefore unacceptable.



Figure 3.8 HPGe detector and shielding at IAC



Figure 3.9 Overhead view of HPGe detector layout at IAC

The positions were marked with letters from A to N; all sample counting for this experiment was placed on either position B or position J. IAC staff members use

calibrated check sources to determine the absolute efficiency of the detector system as a function of energy at each location. This allows researchers to easily convert the results from the HPGe detector for a certain energy into an activity. An example of the pre-made calibration chart for position J is shown below in Figure 3.10. Here we can see the efficiency for the detector peaks around 150 keV, which is very typical for a detector of this type.

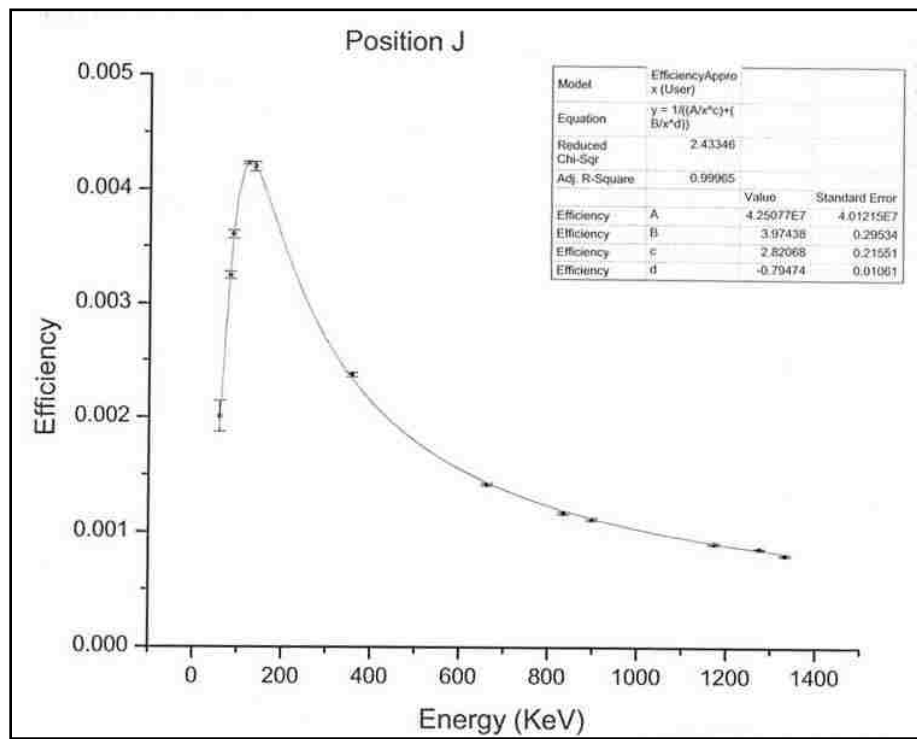


Figure 3.10 IAC supplied efficiency calibration for HPGe detector

The efficiency equation that describes this function is shown below in Equation 3.1. The values of A, B, C and D are experimentally determined for each location. For position J, as an example, the values for A, B, C and D are 4.25E7, 3.97, 2.82 and -0.79, respectively.

$$y(x) = \frac{1}{\left(\frac{A}{x^C} + \frac{B}{x^D}\right)} \quad (3.1)$$

3.4 TARGET MATERIAL AND FORM

The samples were prepared in the radiochemistry labs at the Harry Reid Center at UNLV due to the fact that some of the targets being used were radioactive to begin with. ^{99}Tc is a beta emitter with a half life of 2.11×10^5 years and was prepared by pressing small pellets of Tc metal in a press specifically designed to handle radioactive material. These beads were then placed in the 5N aluminum holders and sealed as described in the earlier chapter.

In order to study the (γ, γ') reaction in Tc, pure Tc metal was used. To study the (γ, n) reaction in ^{19}F , lithium fluoride was used in a powdered form. To study the (γ, α) reactions that produce ^{47}Sc , $^{99\text{m}}\text{Tc}$ and ^{147}Pm , vanadium powder, rhodium powder and europium oxide powder were used, respectively. Finally, gold powder was used to determine and quantify the neutron flux from the irradiation configurations. The masses of each target sample are shown in Table 3.1.

<u>Target</u>	<u>Mass (mg)</u>		<u>Target</u>	<u>Mass (mg)</u>
Tc #1	10.0		EuO #1	53.4
Tc #2	8.1		EuO #2	47.1
Tc #3	8.3		EuO #3	68.5
LiF #1	10.0		Rh #1	48.0
LiF #2	11.1		Rh #2	32.2
LiF #3	9.9		Rh #3	32.0
V #1	108.0		Au #1	79
V #2	118.0		Au #2	74.4
V #3	110.0		Au #3	73

Table 3.1 Masses of the targets used during the irradiation

<u>Irradiation #</u>	<u>Endpoint Energy (MeV)</u>	<u>Beam Time (min)</u>	<u>Targets</u>
1	21	30	Rh #2, LiF #2, V #2, EuO #2
2	23	30	Rh #3, LiF #3, V #3, EuO #3
3	19	30	Rh #1, LiF #1, V #1, EuO #1
4	17	30	Rh #2, LiF #2
5	25	30	Rh #3, LiF #3
6	4	30	Tc #1
7	6	30	Tc #2
8	12	30	Tc #3
9	21	30	Tc #1
10	23	30	Tc #2
11	25	30	Tc #3
12	21	30	Tc #1 with W sideways
13	21	90	Rh #1 #2 #3, LiF #1 #2 #3
14	15	30	Tc #3
15	17	30	Tc #2
16	19	30	Tc #1
17	21	30	Tc #2 & #1 with W coll big (with Au #1 & #2)
18	21	30	Tc #3 with W coll small (with Au #3)
19	21	300	EuO #1 #2 #3, V #1 #2 #3, Rh #1 #2 #3, LiF #1 #2 #3

Table 3.2 Irradiation details for experiments at IAC

CHAPTER 4

MODELING

4.1 STEADY STATE PRODUCTION RATES

For any given activation reaction, it is possible to create a set of equations to describe the expected production rate or loss of the parent, daughter and/or isotope of interest. If, for instance, we were interested in the expected production rate of ^{99m}Tc from natural rhodium targets, we would start with the general form:

$$N_{Rh}(t) = N_{Rh_0}(t)e^{-\int \sigma_{aRh}(E)\phi_{\gamma}(E)(t) dE} \quad (4.1)$$

Where N_{Rh} is the number of rhodium atoms at any given time, N_{Rh_0} is the starting number of rhodium atoms in the target, $\sigma_{aRh}(E)$ is the energy dependant absorption cross section (in this case the (γ,α) cross section), and $\phi_{\gamma}(E)$ is the energy dependant photon flux incident on the rhodium target. This equation describes the loss of rhodium atoms due to the (γ,α) reaction. Now we develop an equation for the production of ^{99m}Tc from this type of reaction. The general form is:

$$\frac{dN_{Tc}}{dt} = \int \sigma_{aRh}(E)\phi_{\gamma}(E)N_{Rh}(t) dE - \int \sigma_{aTc}(E)\phi_{\gamma}(E)N_{Tc}(t) dE - \lambda_{Tc}N_{Tc}(t) \quad (4.2)$$

Now with simple rearrangement we get

$$\frac{dN_{Tc}}{dt} = N_{Rh}(t) \int \sigma_{aRh}(E)\phi_{\gamma}(E)dE - N_{Tc}(t) \int \sigma_{aTc}(E)\phi_{\gamma}(E) dE - \lambda_{Tc}N_{Tc}(t) \quad (4.3)$$

And by combining like terms we see that

$$\begin{aligned}
& \frac{dN_{Tc}}{dt} + N_{Tc}(t) \left(\lambda_{Tc} + \int \sigma_{aTc}(E) \phi_{\gamma}(E) dE \right) \\
&= N_{Rh_0}(t) e^{-\int \sigma_{aRh}(E) \phi_{\gamma}(E) dE} \int \sigma_{aRh}(E) \phi_{\gamma}(E) dE
\end{aligned} \tag{4.4}$$

Now let $\lambda_{Tc_2}(E) = (\lambda_{Tc} + \int \sigma_{aTc}(E) \phi_{\gamma}(E) dE)$ and $\lambda_{Rh_2}(E) = \int \sigma_{aRh}(E) \phi_{\gamma}(E) dE$ in order to form a differential equation that we can solve with an integrating factor. With this substitution, we get

$$\frac{dN_{Tc}}{dt} + \lambda_{Tc_2}(E) N_{Tc}(t) = \lambda_{Rh_2}(E) N_{Rh_0}(t) e^{-\lambda_{Rh_2}(E)t} \tag{4.5}$$

This is now in the general form of

$$y' + P(x)y = Q(x) \tag{4.6}$$

We can use an integrating factor, M

$$M(x) = e^{\int P(x) dx} \tag{4.7}$$

To obtain the general solution of

$$y(x) = \int \frac{M(x)Q(x)dx}{M(x)} \tag{4.8}$$

Given the above,

$$P(x) = \lambda_{Tc_2}(E) \tag{4.9}$$

$$Q(x) = \lambda_{Rh_2}(E) N_{Rh_0}(t) e^{-\lambda_{Rh_2}(E)t} \tag{4.10}$$

$$M(x) = e^{\int \lambda_{Tc_2}(E) dt} = e^{\lambda_{Tc_2}(E)t} \tag{4.11}$$

Now we can solve for N_{Tc} as a function of time

$$N_{Tc}(t) = \int \frac{e^{\lambda_{Tc_2}(E)t} \lambda_{Rh_2}(E) N_{Rh_0}(t) e^{-\lambda_{Rh_2}(E)t} dt}{e^{\lambda_{Tc_2}(E)t}} + C \tag{4.12}$$

By noting that

$$\int e^{-at} dt = -\frac{1}{a} e^{-at} \tag{4.13}$$

We now obtain

$$N_{Tc}(t) = \frac{\lambda_{Rh_2}(E)N_{Rh_0}}{e^{\lambda_{Tc_2}(E)t}} \int e^{-t(\lambda_{Rh_2}(E)-\lambda_{Tc_2}(E))} dt + C \quad (4.14)$$

Integration and simplification gives us

$$N_{Tc}(t) = \frac{\lambda_{Rh_2}(E)N_{Rh_0}}{\lambda_{Rh_2}(E)-\lambda_{Tc_2}(E)} * e^{-\lambda_{Tc_2}t} + C \quad (4.15)$$

Where λ_{Rh_2} , λ_{Tc_2} , and N_{Rh_0} are defined in above equations. To solve for C, we know

that $N_{Tc}(t) = 0$ at time = 0, so by plugging this in we get

$$N_{Tc}(t, t_R) = \frac{\sigma_{aRh}\phi\gamma N_{Rh_0}}{\lambda_{Tc_2}} [1 - e^{-\lambda_{Tc_2}t_R}] e^{\lambda_{Tc_2}t} \quad (4.16)$$

Where t is the time after irradiation and t_R is the irradiation time.

4.2 MCNPX TO PREDICT REACTION RATES

In order to calculate the cross section for a given reaction using the photons from an electron accelerator, the spectrum of that flux must be known. The methods to measure these spectra are extremely complicated; they typically employ various thicknesses of shielding materials with a set of matched detectors. Since this type of equipment is extremely expensive, simulated spectra were created using MCNPX. The Monte Carlo program MCNPX (now called MCNP6) creates the expected photon distribution by following the random interactions that would take place in the electron target, creates the associated photons and transports those photons throughout the geometry of the model. Tally locations are then used to capture the photon flux at various points around the accelerator and geometry. The simulated photon flux for a variety of electron end point energies is found in Figure 4.1.

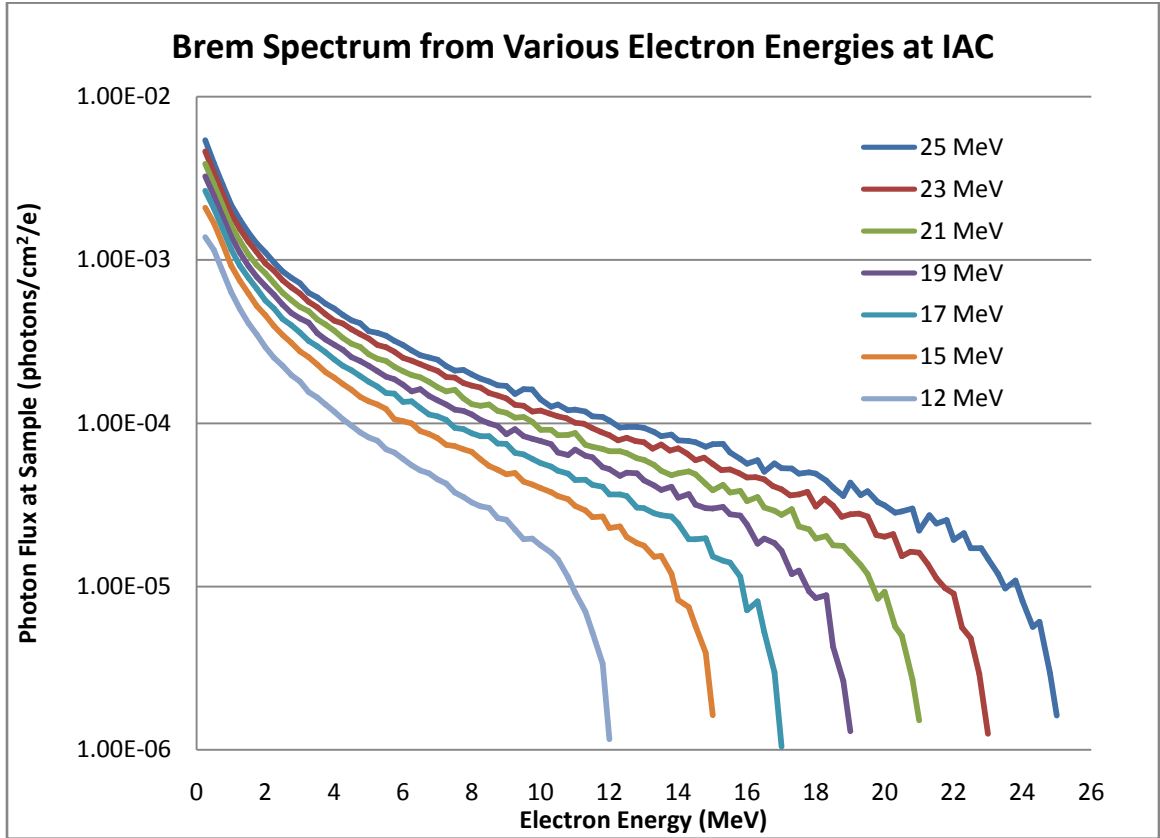


Figure 4.1 MCNPX simulated photon spectra for the IAC LINAC

CHAPTER 5

RESULTS

5.1 MEASURED PRODUCTION RATES

The various target materials described earlier were irradiated for the specified time previously shown in Tables 3.1 and 3.2. The accelerator room was allowed to cool; the length of the cooling period was a function of the irradiation time. The samples were then removed and counted on the HPGe system described in Chapter 3. The total HPGe spectrum acquired for the LiF irradiation at 21 MeV is shown below in Figure 5.1. The line of interest for this isotope is 511 keV since ^{18}F is a positron emitter. A region of interest (ROI) was selected around the 511 lines and then counted in various intervals, depending on activity, other samples to be counted, etc.

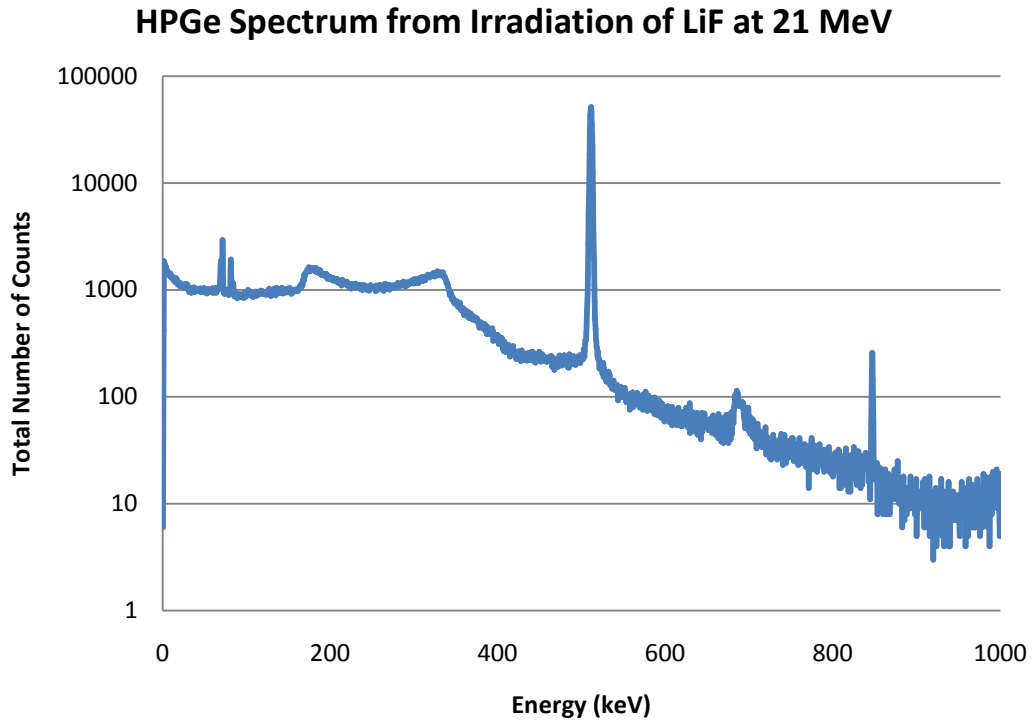


Figure 5.1 HPGe spectrum example from LiF target, 21 MeV

The production of ^{18}F from a lithium fluoride target is shown below. The activity is in units of activity per unit mass, per unit beam power, namely mCi/kg/kW.

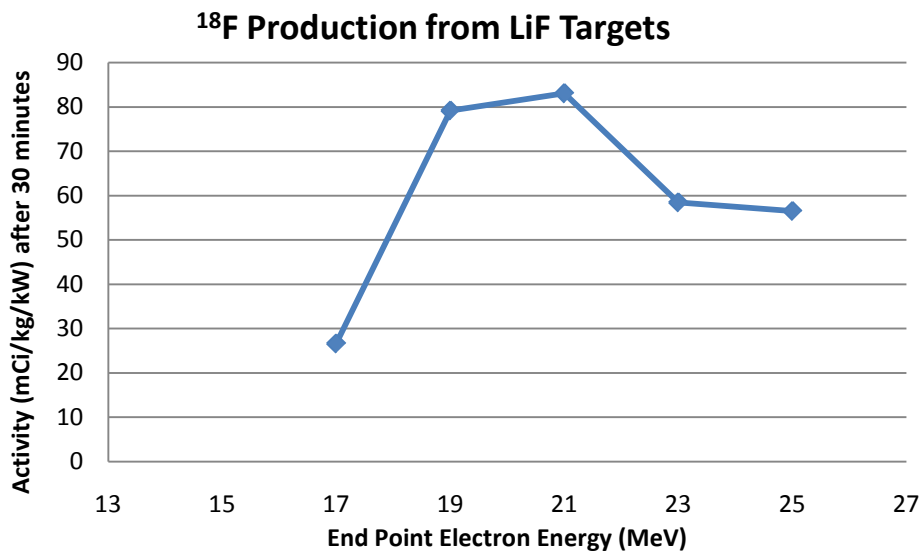


Figure 5.2 ^{18}F production rates from a LiF target

Equilibrium Plot for Creation of ^{18}F from LiF at 21 MeV

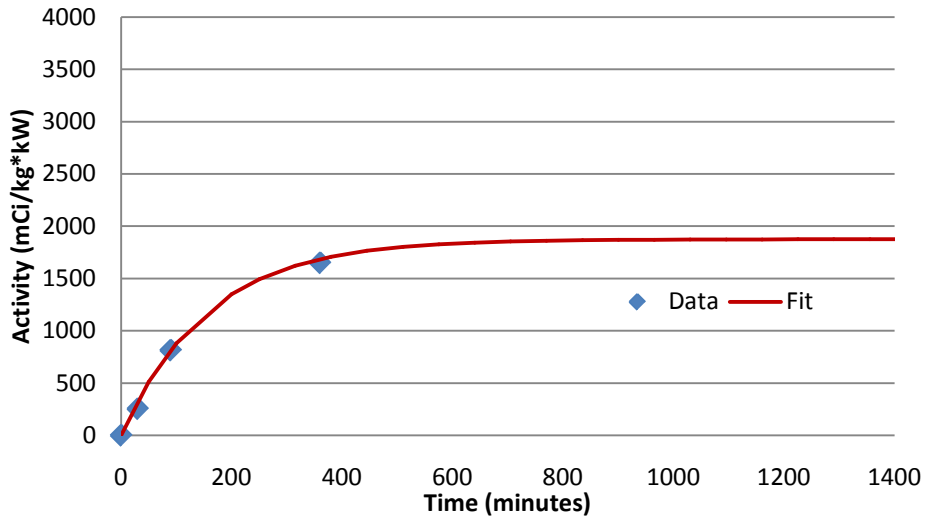


Figure 5.3 Equilibrium plot for ^{18}F from LiF targets

Figure 5.3 shows data from three separate irradiations (the point at zero is implied), namely at 30, 90 and 360 minutes. Here we see good agreement (R^2 values of 0.99) between the four data points and the expected curve fit that describes activation processes.

^{47}Sc Production from V Targets

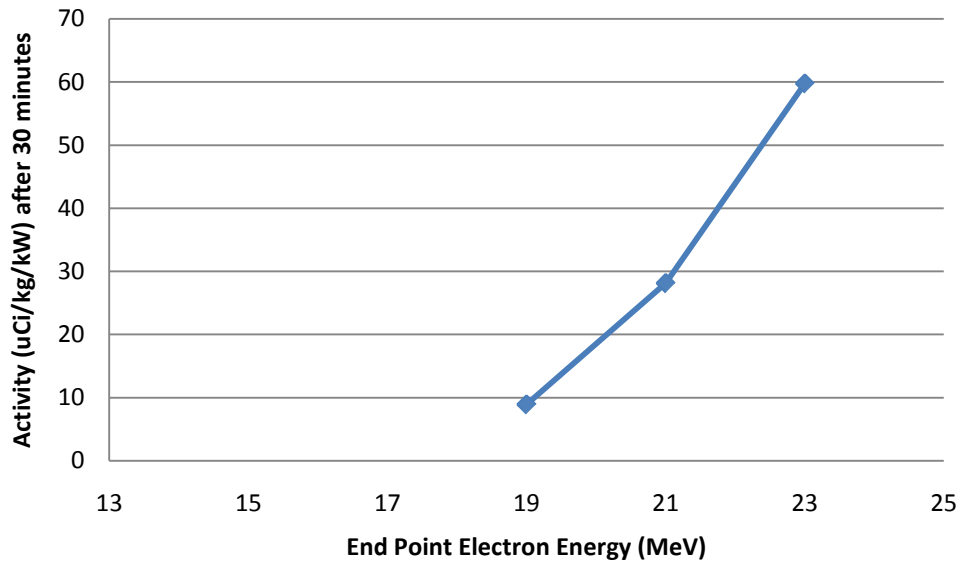


Figure 5.4 ^{47}Sc production from vanadium targets

Figure 5.4 shows the production rate for ^{47}Sc from rhodium targets. Figure 21 shows the equilibrium data and curve fit for this reaction.

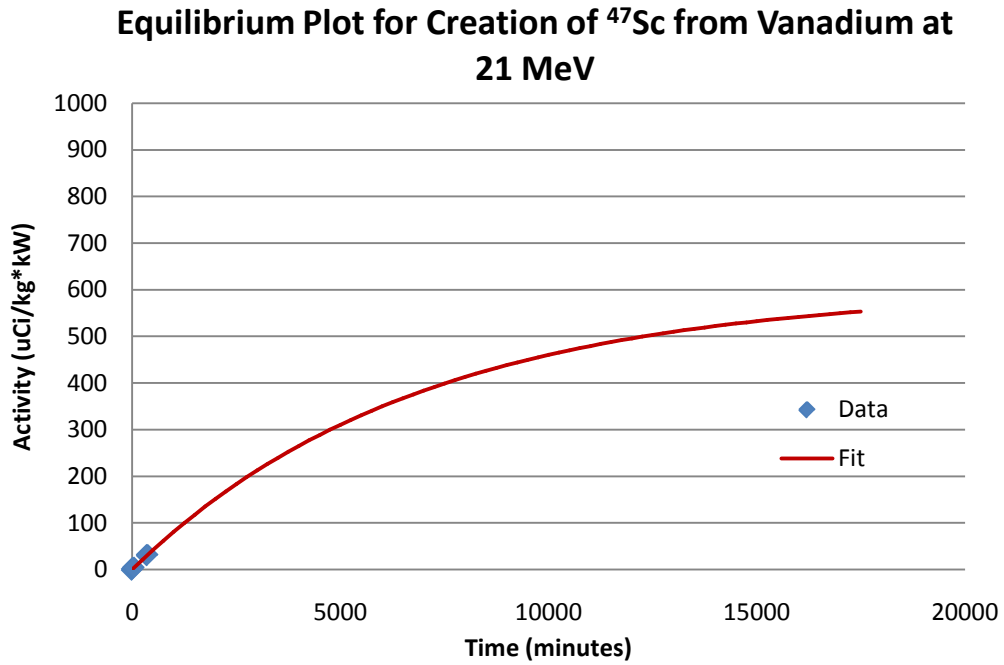


Figure 5.5 Equilibrium data and curve fit for ^{47}Sc from vanadium targets

Figure 5.5 shows the production of $^{99\text{m}}\text{Tc}$ from rhodium powder for a variety of end point energies while Figure 5.6 shows the equilibrium data and curve fit for this reaction.

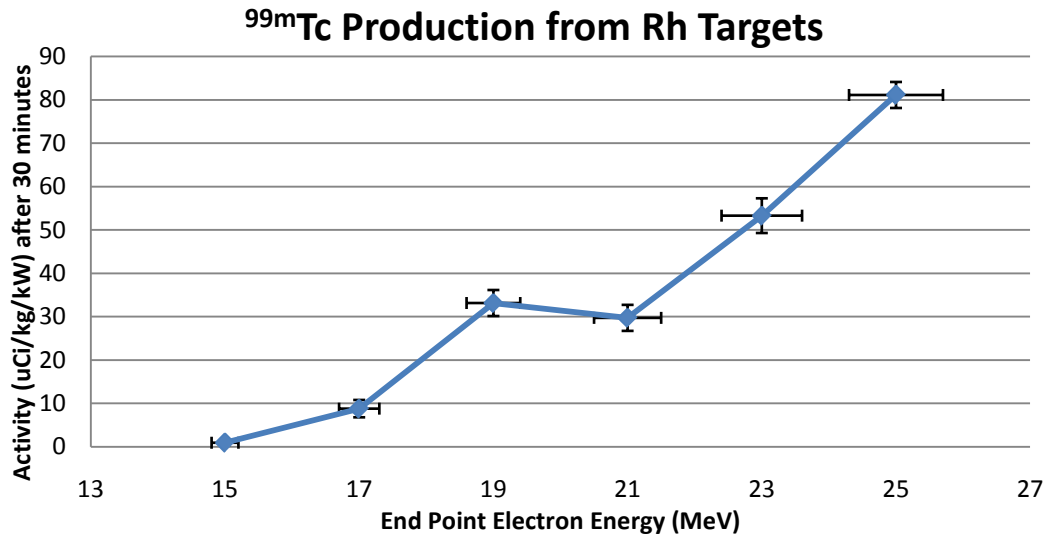


Figure 5.6 Production rates of ^{99m}Tc from rhodium targets

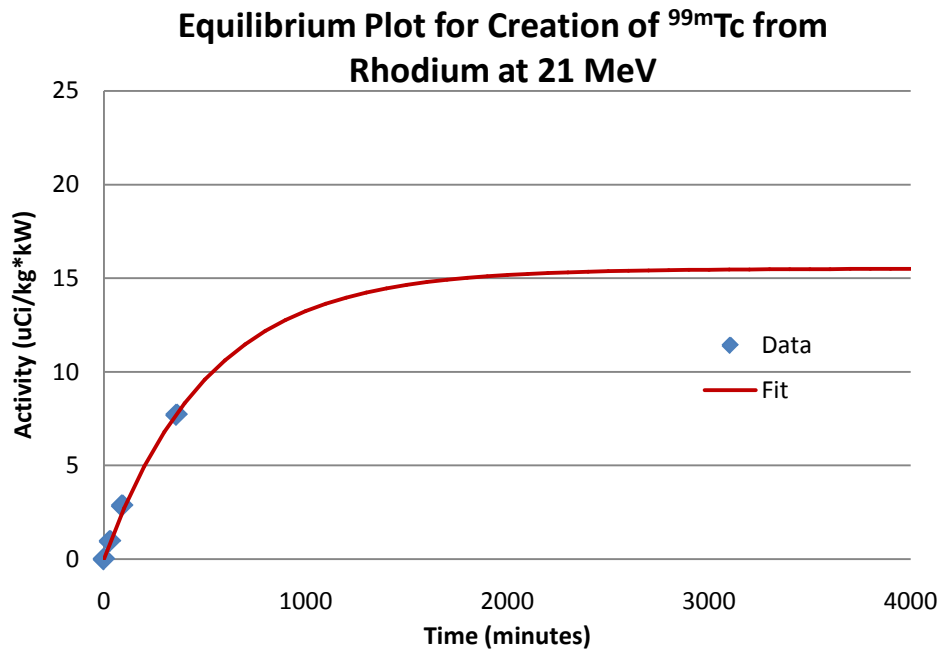


Figure 5.7 Equilibrium data and curve fit for ^{99m}Tc from rhodium targets

Figure 5.7 shows the result of the metastable excitation of ^{99}Tc . The cause of the excited state will be discussed in the conclusions.

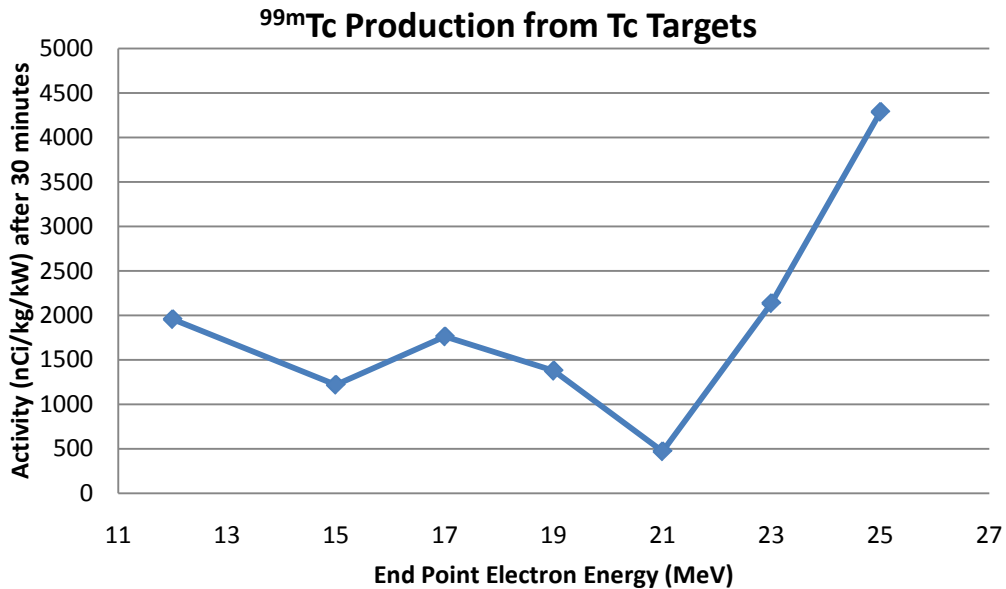


Figure 5.8 ^{99m}Tc production rates from ground state Tc

Figure 5.9 below shows the gold activation that was placed with a few of the samples of ground state Tc during the high energy irradiations. Gold was activated with the Tc samples to prove that the (γ, γ') reaction was indeed causing the excitation in the target. The gold activation provided a means to discount the possibility that the (n, n') reaction was the primary component in the activation process. Low energy and high energy neutrons are present during the irradiation due to the (γ, n) reactions that happen near the bremsstrahlung converter and the surrounding environment. However, the data suggests that the neutron based reactions were a large component of the total activation processes. After an iterative review of the literature on this process, it was noted that not a single paper tried to disprove or quantify the amount of neutrons incident on the target. While it is impossible to quantify the magnitude of each component using this dataset, it may be possible to design an experiment to accurately measure each reaction individually.

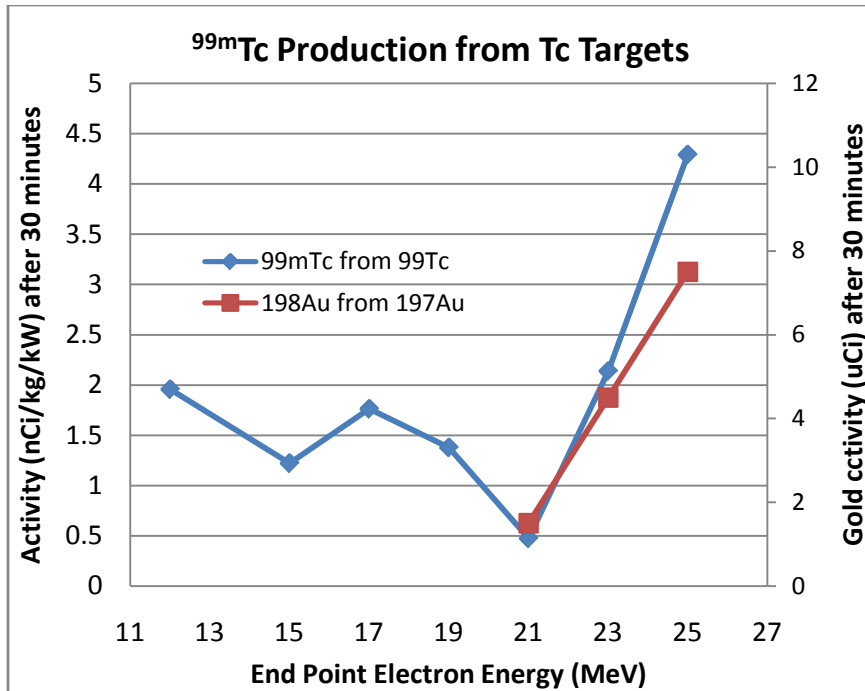


Figure 5.9 Results from gold activation collocated with the Tc samples

5.2 CROSS SECTIONS BASED UPON PRODUCTION RATES

Production rates for each of the radionuclides studied for this work could be computed from equation 2.6 if accurate values of the cross sections, $\sigma(E)$, were known.

Unfortunately, this data has not been available and the experiments discussed in this work were conducted to measure production rates. MCNPX, for example, could be used to approximate production rates based upon the ENDF/B cross section libraries. Since these cross sections are not available in the libraries, the production rates measured for this work were analyzed using the methods described in Section 2.8 to determine the cross sections.

Figure 5.10 shows the cross section for (γ, α) production of ^{99m}Tc from ^{103}Rh targets. The computed cross section has a threshold of 15 MeV. Limited data is available in the ENDF/B cross section libraries for (γ, α) reactions, yet the computed cross sections for ^{103}Rh appear to be consistent with lower Z (aluminum) and higher Z (lead) targets. The resulting cross sections are small with values of about 100 microbarns, (μb), above 23 MeV.

Figure 5.11 provides data on the (γ, n) cross section in ^{19}F . With a threshold energy of about 12 MeV, the cross section peaks at 7.8 mb at 23 MeV.

The (γ, γ') cross section in ^{99}Tc is used to produce ^{99m}Tc and Figure 5.12 shows that this cross section is very small, reaching a minimum of 2.5 μb at 21 MeV to a maximum of 34 μb at 25 MeV.

Limited experimental data was available to compute the (γ, α) to produce ^{47}Sc from ^{51}V , as shown in Figure 5.13. The cross section reached a value of over 600 μb at 25 MeV

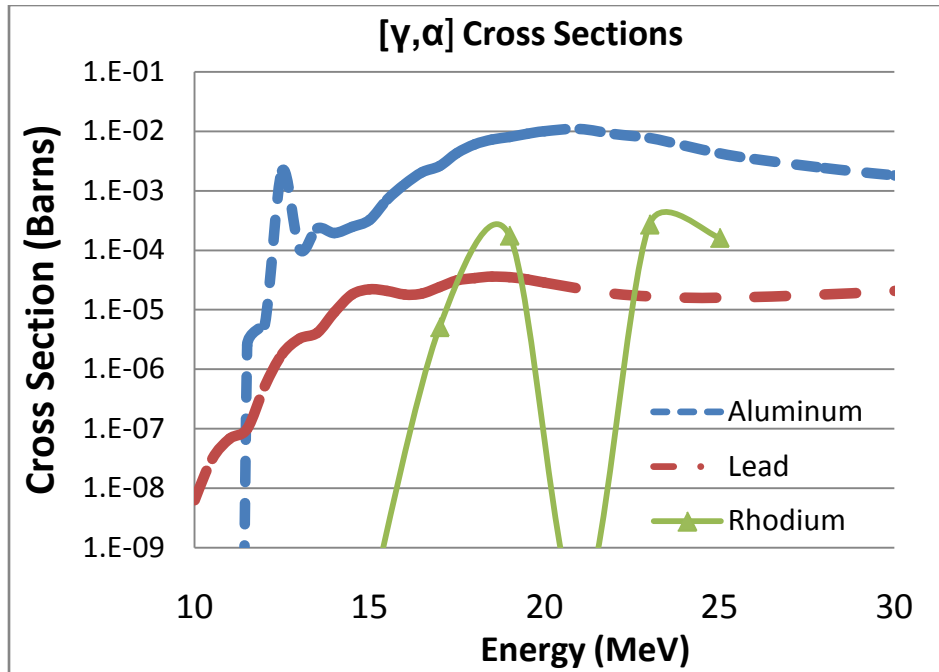


Figure 5.10 [γ, α] Cross section for the production of ^{99m}Tc from ^{103}Rh

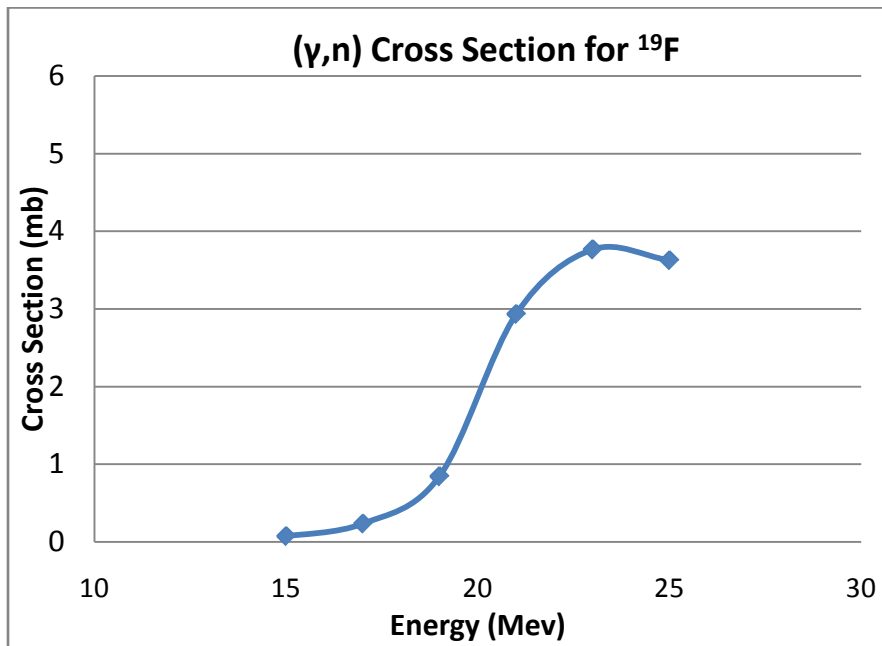


Figure 5.11 [γ, n] Cross section for the production of ^{18}F from ^{19}F

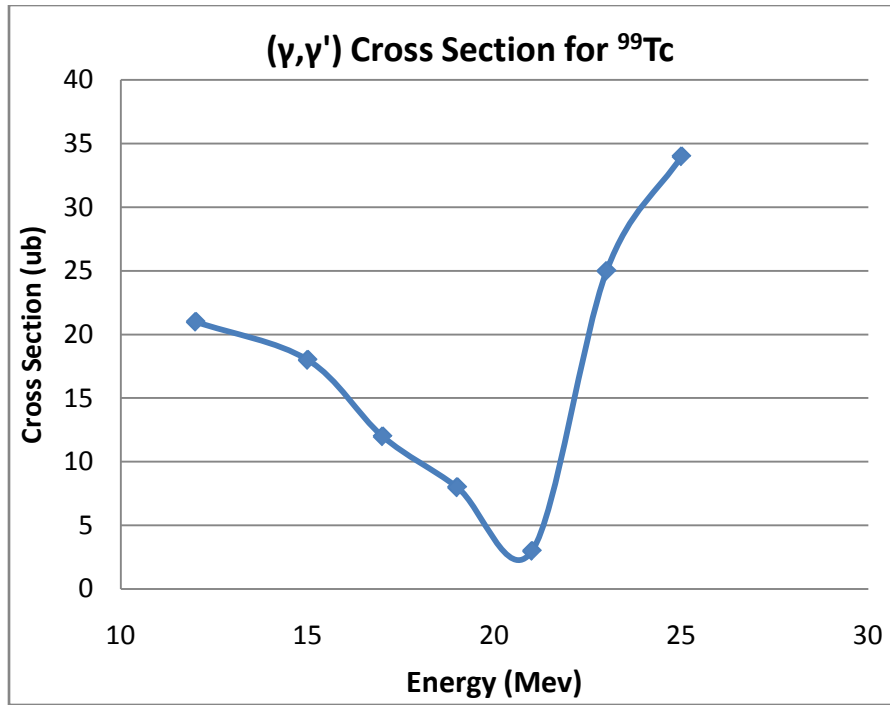


Figure 5.12 [γ, γ'] Cross section for the production of $^{99\text{m}}\text{Tc}$ from ^{99}Tc

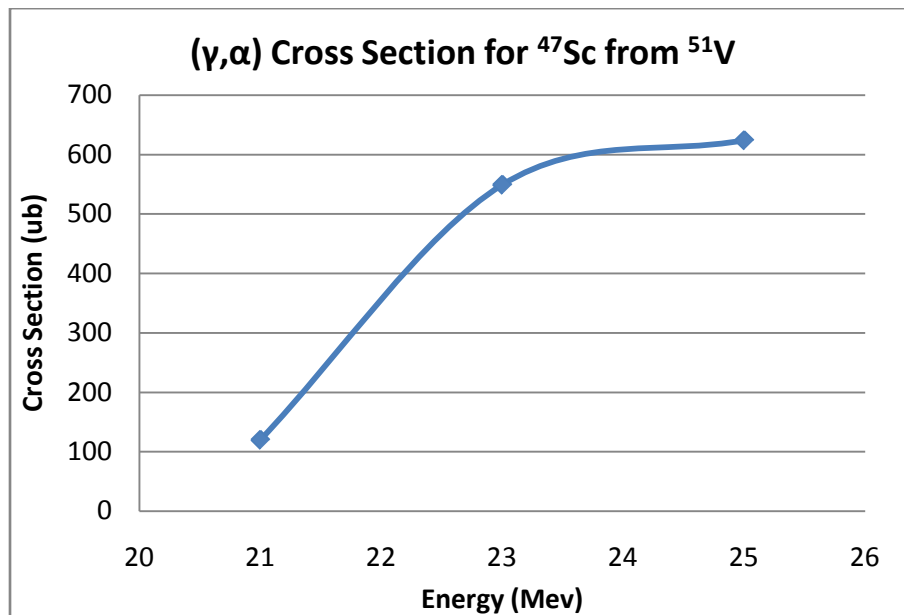


Figure 5.13 [γ, α] Cross section for the production of ^{47}Sc from ^{51}V

CHAPTER 6

CONCLUSIONS

This dissertation was meant to investigate the feasibility of using electron accelerators to produce various radioisotopes for the medical and space communities. While some reactions were primarily used to verify results found in literature (^{18}F from LiF salts), others have never been studied before ($^{99\text{m}}\text{Tc}$ from rhodium and ^{147}Pm from natural europium).

The production of $^{99\text{m}}\text{Tc}$ by excitation from the ground state of Tc shows little promise as an effective method of supplying the medical community with $^{99\text{m}}\text{Tc}$. There are two major issues related to this production method if they were to ever come to market. The first is that one would need a significant amount of Tc metal as the target. Since Tc only comes from spent nuclear fuel, it is unlikely that there would be enough Tc metal to supply the country. Secondly, the target would contain a large majority of Tc with a small amount of $^{99\text{m}}\text{Tc}$. To date, there are no chemical or physical separation techniques that would be able to separate the $^{99\text{m}}\text{Tc}$ from the ground state metal. The only viable way this reaction would work is if the specific activity of the sample were extremely large; this is also highly unlikely due to the low cross section of this reaction. Hence, excitation of Tc metal to the metastable state does not seem to be a likely replacement candidate for $^{99\text{m}}\text{Tc}$ for the medical community.

Furthermore, the activation mechanism for the (γ, γ') is linearly correlated to the neutron activation in gold due to thermal capture that produces ^{198}Au . This can mean one of two things: either the cross section for (γ, γ') process in Tc is the same shape as the thermal neutron absorption cross section for gold, or the activated $^{99\text{m}}\text{Tc}$ is actually from the neutron flux in the room, not the high energy photons. Unfortunately, there is no way to prove this one way or the other. However, it is highly unlikely that the (γ, γ') cross section for any material has the same shape as the thermal neutron absorption cross section for gold, suggesting that the activation here is most likely from neutron activation, namely the (n, n') process.

The production rate of ^{18}F from lithium fluoride salt was primarily conducted to verify the production rate and cross section found in literature. As this is a highly studied process on this element, repeating the experiment gives higher confidence for the reactions that are not as heavily studied. The activation processes produced cross sections that are consistent with the known values found in literature. It was also found that, given the energy ranges studied, 21 MeV produced the most ^{18}F per unit mass per unit beam power, namely $1800 \text{ mCi}/(\text{kg} \cdot \text{kW})$ of ^{18}F from LiF salt in a 600 minute period. This process can create many curies of ^{18}F , however it is an unlikely candidate to replace current technology due to the fact that radioactive ^{18}F and stable ^{19}F are nearly chemically identical, making rapid chemical separation practically impossible. Even though there are ways to mechanically separate the two isotopes, these techniques require very large, very expensive machines, making the viability of this replacement technology low.

The possibility of creating ^{147}Pm from natural europium oxide targets was studied to determine if accelerator based production of this isotope for space applications was feasible. Even though the large majority of space craft use ^{238}Pu as their heat source, the availability of that isotope is becoming quite scarce. As there is no domestic production of this isotope (100% is imported from Russia), ^{147}Pm may be a good alternative given the fact that Russia has told the U.S. they will no longer sell this country ^{238}Pu in the near future. Unfortunately, the amount of ^{147}Pm created from the (γ,α) reaction on ^{151}Eu did not produce a detectable amount of material, even though 1 kW of beam power and high efficiency HPGe detectors were used. This suggests that this method is simply not viable at these energies and these beam currents.

The ability to create ^{47}Sc from vanadium targets seems initially viable by using a 25 MeV LINAC. Since vanadium targets are relatively cheap, the amount of ^{47}Sc that could be created is only limited by engineering constraints as well as self attenuation issues in the target. ^{47}Sc is a viable replacement isotope for ^{177}Lu therapy, but has an added benefit due to the fact it emits a simultaneous 160 keV photon, which could be used in a traditional SPECT scanner. It was proven that approximately 100 uCi/(kg*kW*day) of ^{47}Sc could be produced using a 23 MeV accelerator. Given a 2 kW accelerator and a 10 kg target, this method could produce approximately 2 mCi of ^{47}Sc per day. This amount is enough to support research in the field investigating using this isotope as a replacement for $^{99\text{m}}\text{Tc}$ or ^{177}Lu . There are too many variables to conclude whether or not this production method and amounts would be feasible and/or cost effective in the market place at this time.

Production of ^{99m}Tc from rhodium targets shows high promise in that the production rate is high enough to supply a single large hospital at a price that could potentially be cost effective. At 19 MeV, this method could produce up to 500 mCi per day of ^{99m}Tc given a 2 kW accelerator and a 4 kg target. This production rate is enough to support the daily ^{99m}Tc needs of a large hospital (500-700 beds) assuming the separations technique is both quick and efficient. The concept of separating technetium from a rhodium oxide target can be easily done using aqueous based extraction techniques, but will most likely not be viable in this application due to two main reasons. The first is that the target (all 2 or 3 kg of rhodium oxide) must first be dissolved in an acid, the ^{99m}Tc extracted, and the rhodium be recovered. Even if this process were 99% efficient, a 1% iteration loss per day would be detrimental to the cost of the system. The second reason is that the aqueous based processes would most likely take many hours, if not days, to dissolve, extract, and then reform the target. This would be unacceptable due to the short half life of ^{99m}Tc . It is more likely that a process such as selective volatilization would be a better candidate for this specific application. This process relies on the difference in volatilization properties between technetium oxide and rhodium oxide. This difference would allow the technetium oxide to be volatilized before the target material, liberating it from the target material itself. It could then be transferred away from a target chamber using a carrier gas such as heated carbon dioxide. Further research would need to be conducted before the effectiveness of the entire system could be analyzed.

The ability to produce a variety of unknown cross sections will help future scientists design new types of isotope production facilities using electron accelerators. These cross

section can be used in conjunction with accelerator data, or Monte Carlo simulations, to determine the necessary electron beam and target properties necessary for the desired production rate. Furthermore, this dataset will add to the limited, general scientific database of photonuclear reactions.

APPENDIX I

SAMPLE MCNPX INPUT DECKS

```
IAC 25 mev accelerator input file
c
1 1 -19.0      -1          imp:p,e=1
2 2 -2.0       -2 3 4 1      imp:p,e=1
3 2 -2.0       -5          imp:p,e=1
4 0             -99 #1 #2 #3  imp:p,e=1
5 0             99          imp:p,e=0

c W target
1 RPP -1 1 -1 1 0 0.254
c
c W water jacket
2 RPP -10.16 10.16 -5.08 5.08 -2.54 2.54
3 RPP -1 1 -1 1 -2.54 0
4 RPP -1 1 -1 1 0.254 2.54
c
c Secondary Water jacket
5 RPP -5.08 10.19 -5.08 5.08 3.78 7.59
c
99 RPP -20 20 -20 20 -20 20

mode e p
sdef pos=0 0 -1 erg=25 vec=0 0 1 dir=1 rad=d1 par=e
sil 0 2
spl -21
c
c
f15:p 0 0 12.7 0
e15 0 99i 25
c
nps 1e6
prdmp j 5e4 j j 5e4
c
c
m1 74000 1
m2 13027 90 1001 8 8016 2
```



```

varian X-Ray Source
c
c 6MV beam
c 0.4mm W + 1.5mm Cu Target
c 1.2mm Diameter Circular Beam
c Flux Tally for e/p comparison
c
c Cell Cards
1 0      -1      imp:p,e=1
c 2 4 -7.87 -2 3  imp:p,e=1
10 5 -19    -10    imp:p,e=1
11 6 -8.92 -11    imp:p,e=1
c Collimator impenetrable
12 5 -19      -12 13 imp:p,e=1
13 0          -13    imp:p,e=1
14 5 -19      -14    imp:p,e=1
15 5 -19      -15    imp:p,e=1
c
98 0 1 10 11 12 13 14 15 -98  imp:p,e=1
99 0 98      imp:p,e=0

c Center Sphere
1 SPH 0 0 0 25.6
c
c Truck Body Outside
c 2 RPP -121.92 121.92 -121.92 121.92 -304.8 304.8
c
c Truck Body Inside
c 3 RPP -121.42 121.42 -121.42 121.42 -304.3 304.3
c
c W Target (0.4mm)
10 RPP -3.28 3.28 577.15 577.19 -2.5 2.5
c
c Cu Target (1.5mm)
11 RPP -3.28 3.28 577 577.15 -2.5 2.5
c
c Lead Collimator (9cm lead) 1.2mm beam width
12 RPP -10 10 568 577 -10 10
13 RPP -3.28 3.28 568 577 -.06 .06
c Additional collimator piece(s) 18cm thick
14 RPP -10 10 550 568 .06 10
15 RPP -10 10 550 568 -10 -.06
c
c Environment
98 BOX -150 -150 -404.8 300 0 0 0 750 0 0 0 809.6

DBCN 7j 10789123456789
SSW 12.4 (98)
c
mode p e
nps 5e8
prdmp j 5e8 j j 5e8
cut:e j .05
cut:p j .05
c

```

```

c 1.2mm Diameter Electron Beam
SDEF pos 0 596 0 vec 0 1 0 dir -1 axs=0 1 0 rad=d1 ext=0 erg=d3 par=e
sil 0 .06
sp1 -21
c
c Gaussian Energy Spectrum (Mean 9MeV FWHM=150keV 20keV bins)
si3 8.80 8.82 8.84 8.86 8.88 8.90 8.92 8.94 8.96 8.98 9.00 9.02 9.04
9.06
      9.08 9.10 9.12 9.14 9.16 9.18 9.20
sp3 d 0 .001511 0.003644 0.00797 0.016 0.028 0.046 0.069 0.092 0.112
0.123
      0.123 0.112 0.092 0.069 0.046 0.028 0.016 0.00797 0.003644
0.001511
c
c Tungsten (density=19.25 g/cc)
m5 74000 -1.00
c
c Copper (density=8.920 g/cc)
m6 29000 -1.00
c
c Lead (density=11.340 g/cc)
c m7 82000 -1.00
c
print

```

APPENDIX II

DIFFERENTIAL EVOLUTION PROGRAM

```
      E = 0
      ' generated by the accelerator.
      ' A.1 This is the energy of the monochromatic electrons
      E0 = Accelerator_Electron_Energy(k)      ' (MeV).
for k=0 to (D - 1)

'-----
--
'
' Program:  obj-steps.bas
'
' Purpose:  This program is used to calculate the x-ray fluence as
'           a function of energy for an electron accelerator and a
'           bremsstrahlung target.
'
' Status:
'-----
--

' 1.  Function declarations.

      declare function set_up_constants() as integer

      declare function integral(number_of_intervals as integer, x() as
double, _
                               f() as double) as double

      declare function sigma_Rh103(D as integer, A() as double, _
                                   E as double) as double

      declare function objective_function(NN as integer, D as integer,
vector() _
                                         as double) as double

      declare function psi_fake(E_electron as double, E_xray as double) as
double

' 2.  Shared variables and definition of function "psi" for
bremstrahlung data.

      dim shared as integer NNN = 500, number_of_brem_samples,
brem_data_loaded = 0
      dim shared as double Brem_psi(7,NNN), Brem_energy(NNN)

      declare function psi(E_electron as double, E_xray as double) as
double
```

```
' 3. Shared constants dealing with the irradiation and the
accelerator.
```

```
dim shared as double t_irradiation, t_post_irradiation, Z
dim shared as double accelerator_power
dim shared as double Accelerator_Electron_Energy(10)
dim shared as double Measured_Tc99m_Activity(10)
dim shared as double lambda_2, lambda_2T, lambda_1T, N_10, _
t_half-life_Tc99m, m_Rh103
```

```
' 4. Shared constants and unit conversions.
```

```
dim shared as double joules_per_MeV = 1.602E-13 ' (MeV/J).
dim shared as double Bq_per_microcurie = 3.7e4 '
(Bq/microcurie).
dim shared as double Avogadro = 6.023e23 '
(atoms/gmole).
dim shared as double A_Rh103 = 103.0 ' (g/mole).
dim shared as double barns_per_cm2 = 1.0e24 ' (b/cm^2).
dim shared as double CEILING = 1e25
```

```
function set_up_constants() as integer
```

```
dim as integer i, k

'-----
'
' A. Define the measured radioactivity of the Tc-99m samples
' as a function of the peak accelerator energy.
'
' 1. Measured electron energies in (MeV).
' 2. Measured activity of Tc-99m in (microcuries/(kg*kW)).
'-----

Accelerator_Electron_Energy(0) = 12
Measured_Tc99m_Activity(0) = 0.00 * Bq_per_microcurie

Accelerator_Electron_Energy(1) = 15
Measured_Tc99m_Activity(1) = 0.00 * Bq_per_microcurie

Accelerator_Electron_Energy(2) = 17
Measured_Tc99m_Activity(2) = 26.69 * Bq_per_microcurie

Accelerator_Electron_Energy(3) = 19
Measured_Tc99m_Activity(3) = 51.40 * Bq_per_microcurie

Accelerator_Electron_Energy(4) = 21
Measured_Tc99m_Activity(4) = 71.50 * Bq_per_microcurie
```

```

Accelerator_Electron_Energy(5) = 23
Measured_Tc99m_Activity(5)     = 106.66 * Bq_per_microcurie

Accelerator_Electron_Energy(6) = 25
Measured_Tc99m_Activity(6)     = 175.67 * Bq_per_microcurie

```

```

-----
'
' B. Define specifications for the electron accelerator and
' the bremsstrahlung source.
'
'-----
-----

```

```

target.      Z                = 74      ' Tungsten bremsstrahlung

```

```

accelerator_power = 1000      ' (watts).

```

```

' C.1 This information pertains to the rhodium target
' and irradiation specifications.

```

```

t_irradiation    = 30 * 60      ' (s).

```

```

t_post_irradiation = 5 * 60     ' (s).

```

```

t_half-life_Tc99m = 6.0058 * 3600 ' (s).

```

```

' C.2 How many Rh-103 atoms are there to begin with?

```

```

m_Rh103         = 1            ' (kg).

```

```

return 0

```

```

end function

```

```

function objective_function(NN as integer, D as integer, A() as double)
as double

```

```

dim as double SE, SE_sum, Eo, E, max_fluence, G_total
dim as double sigma(NN), f(NN), energy(NN), dFLUXdE(NN)
dim as double N_2, A_Tc99m

```

```

dim as integer i, j, k

```



```

-----
for i=0 to (NN-1)
  f(i) = sigma(i) * dFLUXdE(i) / barns_per_cm2
next i

' C.1 Energy is in units of MeV and f() = sigma * dFlux/dE
is in
' photons/(MeV*sec).

lambda_1T = integral(NN, energy(), f())
lambda_2 = log(2)/t_half-life_Tc99m
lambda_2T = lambda_2

-----
'
' D. Calculate the objective function based on the standard
' error between the measured sample radioactivity versus
' the values predicted from the Breit-Wigner distribution.
'
-----

' D.1 Compute the radioactivity of the Tc99m based on the
' absorption cross section.

' D.1.a The original number of Rh-103 atoms is N(10).
N_10 = m_Rh103 * Avogadro / (A_Rh103/1000) '
(atoms/m^3).

' D.1.b The number of Tc-99m atoms as a function of time,
N_2.

N_2 = ((lambda_1T * N_10)/(lambda_1T - lambda_2T))
* _
(exp(-lambda_2T * t_irradiation) - _
exp(-lambda_1T * t_irradiation)) * _
exp(-lambda_2 * t_post_irradiation)

' D.1.c Radioactivity of the Tc-99m inventory.

A_Tc99m = lambda_2 * N_2 ' (Bq).
if A_Tc99m < 0 then A_Tc99m = 0.0

' D.1.d Accumulate the sum of the deviation between
measured and
' computed radioactivity of the sample, due to Tc-
99m.

SE_sum += (A_Tc99m -
Measured_Tc99m_Activity(k))^(2.0)
'print "obj: k, SE_sum, A_Tc99m, Measured = "; k, SE_sum, A_Tc99m,
Measured_Tc99m_Activity(k)

```

```

next k

    SE = sqr(SE_sum)

    ' print "    SE          = "; SE
    ' print

'print "obj:  SE = "; SE

' input i

return SE

end function

```

```

function sigma_Rh103(D as integer, A() as double, E as double) as
double

```

```

-----
-
'
' Function:  sigma_Rh103
'
' Purpose:  Return the [gamma, alpha] spectrum for Rh-103
'           based on an array of Breit-Wigner (BW) peaks.
'
' Input:    1) D    = Number of steps.
'           2) A()  = Values of cross section in each step.
'           3) E    = energy of the incident photon, (MeV).
'
' Output:   1) sigma_Rh103 = [gamma, alpha] cross section, (b).
'
-----
-

```

```

dim as double value

```

```

if (          (E <= 12)) then value = A(0)
if ((E > 12) and (E <= 15)) then value = A(1)
if ((E > 15) and (E <= 17)) then value = A(2)
if ((E > 17) and (E <= 19)) then value = A(3)
if ((E > 19) and (E <= 21)) then value = A(4)
if ((E > 21) and (E <= 23)) then value = A(5)
if ((E > 23)          ) then value = A(6)

```

```

return(value)

```



```
end function
```

```
function integral(number_of_intervals as integer, x() as double, _  
                  f() as double) as double
```

```
-----  
'  
'  
' Function: integral  
'  
' Purpose: This function will integrate the given function from  
the lower limit of the independent variable to the upper limit  
' with the requested number of iterations. This reports the  
integral of f(i) over x(i).  
'  
' Input:  
'  
' a) f(i) - an array describing the variable to be  
integrated as a function of x(i), for i = 0 to  
"number_of_intervals."  
' b) lower_limit - lower limit of the independent variable.  
' c) upper_limit - upper limit of the independent variable.  
' d) number_of_intervals - this is the number of intervals that  
the independent variable is divided into.  
'  
' Output:  
'  
' a) integral() - the value of the integral is returned as a  
double.  
'  
-----  
-----
```

```
dim as integer N, i  
dim as double h, sum, result, dx  
dim as double lower_limit, upper_limit  
  
N = number_of_intervals  
  
dx = (x(N-1) - x(0))/N  
  
sum = 0.0  
for i=0 to (N - 1)  
    sum += f(i) * dx  
next i  
result = sum  
  
' h = (x(N-1) - x(0)) / N
```

```

'         sum = f(0)
'
'         for i=1 to (N - 3) step 2
'             sum += 4 * f(i)
'         next i
'
'         for i=2 to (N - 2) step 2
'             sum += 2 * f(i)
'         next i
'
'         sum += f(N-1)
'
'         result = (h * sum / 3)
'
return result

```

end function

```
function psi_fake(E_electron as double, E_xray as double) as double
```

```

if (E_electron = 25.0) then return 0.0003501058/25.0
if (E_electron = 23.0) then return 0.0003271052/23.0
if (E_electron = 21.0) then return 0.0002973088/21.0
if (E_electron = 19.0) then return 0.0002727925/19.0
if (E_electron = 17.0) then return 0.0002469449/17.0
if (E_electron = 15.0) then return 0.0002169186/15.0
if (E_electron = 12.0) then return 0.0001714793/12.0

```

end function

```
function psi(E_electron as double, E_xray as double) as double
```

```

dim as double value, E_min, E_max, position
dim as string inline
dim as integer i, j, k, n

```

```

'-----
-----
'
' Function: psi
'
' Purpose: This function yields the number of photons generated
per
'         cm^2 of target area per electron per MeV from
Danny's
'         MCNPX simulations of the IAC accelerator. The input
data

```

```

'           includes the maximum accelerator voltage (electron
energy)
'           and for the requested x-ray energy.
'
Notes:  1)  If the raw data hasn't been read in from disk,
do it
'           when this function is first called.
'
'           2)  Based on the electron energy, choose the correct
vector
'           of solutions.
'
'           3)  Next, interpolate between values in the vector
based
'           upon the indicated xray energy.
'
Input:  1)  E_electron - accelerator electron energy, (MeV).
'           2)  E_xray   = the value of psi is found for the
'           requested xray energy and reported,
(MeV).
'           3)  Disk file "Dannys-Bremsstrahlung_Data.txt"
'
Output: 1)  psi       = the bremsstrahlung production rate
in
'           photons per (cm^2 * electron *
MeV).
'
-----

```

```

if (brem_data_loaded = 0) then
'   print "Bremsstrahlung data has been read in."
'   open "Dannys-Bremsstrahlung_Data.txt" for input as #1
'   Read in the bremsstrahlung data from disk.
'
'   j = 0
do
'
'   line input #1, inline
'
'   n = 0
for i=1 to len(inline) step 9
'
'   if i = 1 then
'       Brem_energy(j) = val(mid(inline, i, 9))
'   else
'       Brem_psi(n-1, j) = val(mid(inline, i, 9))
'   end if
'
'   n += 1
'
next i
'
'   j += 1

```

```

loop until (eof(1) = -1)

    number_of_brem_samples = j

    close #1

    brem_data_loaded = 1

end if

' Now, select the correct vector based on the electron energy and
' interpolate the value of "i" to the correct energy value in the
vector.

E_min = 0
E_max = 25

if (E_electron = 25.0) then j = 0
if (E_electron = 23.0) then j = 1
if (E_electron = 21.0) then j = 2
if (E_electron = 19.0) then j = 3
if (E_electron = 17.0) then j = 4
if (E_electron = 15.0) then j = 5
if (E_electron = 12.0) then j = 6

    position = ((number_of_brem_samples-1) * E_xray)/(E_max -
E_min)
    i      = int(position)

    if (i > number_of_brem_samples - 1) then
        value = 0.0
    else
        value = Brem_psi(j,i) + (Brem_psi(j,i+1) -
Brem_psi(j,i)) * (position - i)
    end if

    return value

end function

```

```

#include "obj-steps.bas"

dim MAX_DATA_PAIRS as integer, MAX_DIMENSIONS as integer
  MAX_DATA_PAIRS    = 2000    ' Maximum number of data pairs.
  MAX_DIMENSIONS    = 5      ' Maximum number of dimensions
                          ' (independent variables).

dim as double x(MAX_DIMENSIONS,MAX_DATA_PAIRS), y(MAX_DATA_PAIRS), _
  y_computed(MAX_DATA_PAIRS), eta(MAX_DATA_PAIRS)
dim eta_max as double
dim maxorder as integer, nitems as integer, dimensions as integer
dim i as integer, j as integer, k as integer, index as integer
dim NP as integer, D as integer
dim a_upper as double, a_lower as double
dim F as double, CR as double
dim minimum_cost as double, index_min_cost as integer, best_index as
integer
dim generation as integer, max_generations as integer
dim r1 as integer, r2 as integer, r3 as integer
dim as integer n, L
dim as double sum, trial_cost, mean_cost, cost_standard_error
dim debug as integer
dim tolerance as double
dim input_line as string
dim start_time as double, stop_time as double, max_runtime as double
dim notification_timer as double, completion_percentage as integer

  dim as integer NN = 1001    ' This is the number of energy
increments used to          ' calculate cross-section.

  dim as double SE_sum, Eo, E
  dim as double ff(NN), sigma(NN), dFLUXdE(NN), energy(NN)
  dim as double A_Tc99m, N_2

  dim as integer ii

'-----
'
' PROGRAM:  DE-STEPS.BAS
'
' PURPOSE:  This program is developed to calculate the optimal
coefficients
'           in a vector "a" based on a differential evolution
algorithm.
'
' Input:    1) data.dat - file containing pairs of data to be fitted.
'           2) input.txt - user data input file.
'           3) external function containing the objective function
for the run.
'

```

```

' Output:  1) text to screen containing results of the run.
'          2) optional debugging output as text to screen.
'
' Version: 1, 5/26/2011, wgc
'          2, 1/30/2012, modified for multiple independent variables.
'          3, 6/14/2012, modified for Danny's data from the IAC.
'          4, 10/15/2012, modified for discrete cross-section groups
(7 steps).
'
'-----
'-----

```

```

'-----
'
' A. Read in initial data.
'-----
'-----

```

```

open "fit-output.dat" for output as #5

'print "main: A"
' A.1 Read in user data from 'input.txt.'

open "input-steps.txt" for input as #1

do while(eof(1) = 0)

    line input #1, input_line

    if mid(input_line,8,3) = "A.1" then maxorder =
int(val(mid(input_line,70,10)))
        D = 7

    if mid(input_line,8,3) = "A.2" then tolerance =
val(mid(input_line,70,10))
        if mid(input_line,8,3) = "A.3" then dimensions =
int(val(mid(input_line,70,10)))

    if mid(input_line,8,3) = "B.1" then NP =
int(val(mid(input_line,70,10)))
        if mid(input_line,8,3) = "B.2" then F =
val(mid(input_line,70,10))
        if mid(input_line,8,3) = "B.3" then CR =
val(mid(input_line,70,10))

    if mid(input_line,8,3) = "C.1" then debug =
int(val(mid(input_line,70,10)))
        if mid(input_line,8,3) = "C.2" then max_generations =
int(val(mid(input_line,70,10)))
        if mid(input_line,8,3) = "C.3" then max_runtime =
val(mid(input_line,70,10))

```

```

        max_runtime *= 60 ' Convert from minutes into seconds to
be compatible with 'timer.'

    loop

        close #1

' A.2 Define the experimental data to be compared with the
'   calculated values.

        set_up_constants()

'-----
'
' B. Initialization
'-----
'-----
'print "main: B"

        dim c(NP, D) as double, cost(NP) as double, c_vector(D) as double
        dim best_vector(D) as double, value as double
        dim as double mutation_vector(D), old_ensemble(NP,D),
new_ensemble(NP,D)
        dim a(D) as double

' B.1 Make random guesses for the solution vectors assembled
into "NP" populations.

        randomize timer
        print rnd

        for i=0 to (NP-1)

            for j=0 to (D - 1)
                c(i,j) = rnd * 10^(-4)
                c_vector(j) = c(i,j)
            next j
            cost(i) = objective_function(NN, D, c_vector())
        next i

' B.2 Find the minimum objective function for these guessed
solution vectors.

        minimum_cost = cost(0)
        for i=0 to (NP-1)
            if(cost(i) < minimum_cost) then
                minimum_cost = cost(i)
                index_min_cost = i
            end if

```

```

next i

' B.3 Now, move the best solution vector into "best_vector" and
store the index.

    for j=0 to (D-1)
        best_vector(j) = c(index_min_cost,j)
    next j
    best_index = index_min_cost

' B.4 Move the ensemble "c(NP,D)" into the "old" ensemble.

    for i=0 to (NP-1)
        for j=0 to (D-1)
            old_ensemble(i,j) = c(i,j)
            new_ensemble(i,j) = c(i,j)
        next j
    next i

'-----
'
' C. Process through each generation of optimal solutions.
'-----

'print "main: C"

    start_time          = timer
    notification_timer  = 0
    generation          = 0
    completion_percentage = 0

' C.1 Notify the user as to the expected completion time.

    print "Job started at: ";time;" with a maximum runtime of:
";max_runtime/60;" (min) or: ";_
        max_generations; " generations."
    print "Job Completion: 00 % at ";time;" with zero
generations."

    while ((generation < max_generations) and ((timer - start_time) <
max_runtime))

        generation += 1

        ' Let the user know how much is completed every 10% of the
max. runtime.

```



```

        notification_timer = timer - (start_time +
completion_percentage*max_runtime/100)
        if (notification_timer > max_runtime/10) then
            completion_percentage += 10
            print "Job Completion: ";completion_percentage;" % at
";time;" with ";generation;_
                " generations and performance ratio of:
";((mean_cost - tolerance)/tolerance);"."
            notification_timer = 0
        end if

        if (debug = 1) then
            print "
            print "Generation = ", generation;"/";max_generations;" (D,
NP) = ";D, NP
        end if

' C.2 Pick 5 random integers to refer to different
populations (out of NP).

'print "main: C.2"

    for i=0 to (NP-1)

        do
            r1 = rnd * (NP-1)
            if (r1 <> i) then exit do
        loop

        do
            r2 = rnd * (NP-1)
            if(r2 <> i and r2 <> r1) then exit do
        loop

        do
            r3 = rnd * (NP-1)
            if(r3 <> i and r3 <> r2 and r3 <> r1) then exit do
        loop

        if (debug=1) then
            print "    i, r1, r2, r3 = ", i, r1, r2, r3
            print "
            end if

'print "main: C.3"

' C.3 Complete the Differential Evolution (DE) strategy.
Replace elements of the best
' vector to form a new mutation vector.

    for j=0 to (D-1)
        mutation_vector(j) = old_ensemble(i,j)
        if (mutation_vector(j) < 0.0) then mutation_vector(j) =
0.0

```

```

        next j

        n = rnd * (D-1)
'print "main: C.3.5"
        L = 0
        do
            mutation_vector(n) = old_ensemble(r1,n) + F *
(old_ensemble(r2,n) - old_ensemble(r3,n))
            if (mutation_vector(n) < 0.0) then mutation_vector(n) = 0.0
'print "main: L = ";L
            if (debug=1) then
                print "    mutation_vector(";n;")    =
";mutation_vector(n)
                print "    best_vector(n)          = ";best_vector(n)
                print "    old_ensemble(";r2;","n)    =
";old_ensemble(r2,n)
                print "    old_ensemble(";r3;","n)    =
";old_ensemble(r3,n)
                print "    n, L, mutation_vector(n) =
";n,L,mutation_vector(n-1)
            end if

            n          = (n+1) mod (D)
            L          += 1

        loop while ((rnd < CR) and (L < D))

'print "main: C.4"

' C.4 Try the mutation to see how well it works.

        trial_cost = objective_function(NN, D, mutation_vector())

        if (debug=1) then print "    Trial_cost = ", trial_cost

        if (trial_cost <= cost(i)) then

            cost(i) = trial_cost

            for j=0 to (D-1)
                new_ensemble(i,j) = mutation_vector(j)
            next j

            if (trial_cost < minimum_cost) then
                minimum_cost = trial_cost
                index_min_cost = i

                for j=0 to (D-1)
                    best_vector(j) = mutation_vector(j)
                next j

            end if

```

```

else
    for j=0 to (D-1)
        new_ensemble(i,j) = old_ensemble(i,j)
    next j

end if

next i ' End the mutation loop.

'print "main: C.5"

' C.5 Swap ensembles replacing the new generation with the
old one.

    for k=0 to (NP-1)
        for j=0 to (D-1)
            value = old_ensemble(k,j)
            old_ensemble(k,j) = new_ensemble(k,j)
            new_ensemble(k,j) = value
        next j
    next k

'print "main: C.6"

' C.6 Compute the mean and the variance of the objective
"cost" function.

    sum = 0
    for j=0 to (NP-1)
        sum += cost(j)
        if (debug=1) then print "    cost(";j;") = ",cost(j)
    next j
    mean_cost = sum/NP

    sum = 0
    for j=0 to (NP-1)
        sum += (cost(j) - mean_cost)^2
    next j
    cost_standard_error = sqr(sum/(NP-1))

    if (debug = 2) then
        print "    generation, mean_cost, %st.error = ",
generation, mean_cost, cost_standard_error*100/mean_cost
    end if

    if (mean_cost < tolerance) then exit while

    if (debug = 3) then
        print "main: generation, mean_cost = ";
generation, mean_cost
    end if

```

```

'-----
'
' Print out the best vector to a disk file titled:  "fit-
output.dat"
' The order of the data stored in fit-output.dat is:
'
'     generation
'     a(0)
'     ...
'     a(D-1)
'     minimum_cost
'-----

print #5, generation; " ";

for i=0 to (D-1)
  print #5, best_vector(i); " ";
next i

print #5, minimum_cost

print "gen/cost= "; generation, minimum_cost

wend

stop_time = timer

close #5

'-----
'
' D. Print out the results.
'-----

open "output.doc" for output as #3
open "sigma-Rh103.txt" for output as #4

print #3, "
"
print #3, "-----"
---"
print #3, "|
|"
print #3, "|           Differential Evolution Results
|"
print #3, "|
|"
print #3, "-----"
---"

```

```

    print #3, "
"
    print #3, " A. Print out the coefficients of the curvefit.
"
    print #3, "     A.1 Maximum order of fit:                ";
D
    print #3, "     A.2 Cross Section (b):
"
    print #3, "           0 <= E(MeV) < 12 :                ",
best_vector(0)
    print #3, "           12 <= E(MeV) < 15 :                ",
best_vector(1)
    print #3, "           15 <= E(MeV) < 17 :                ",
best_vector(2)
    print #3, "           17 <= E(MeV) < 19 :                ",
best_vector(3)
    print #3, "           19 <= E(MeV) < 21 :                ",
best_vector(4)
    print #3, "           21 <= E(MeV) < 23 :                ",
best_vector(5)
    print #3, "           23 <= E(MeV) < 25 :                ",
best_vector(6)
    print #3, "
"
    print #3, " B. Print out the table for the fit.
"

    SE_sum = 0

    for k = (D - 1) to 0 step -1

        Eo = Accelerator_Electron_Energy(k)           ' (MeV).

        ' A.1 This is the energy of the monochromatic electrons
        ' generated by the accelerator.

        E = 0
        for i = 0 to (NN-1)
            energy(i) = E                               ' (MeV).
            dFLUXdE(i) = psi(Eo, E) * accelerator_power / _
                (Eo * joules_per_MeV)                 '
        (photons/cm^2 * s).
            E += Eo/NN
        next i

        '-----
        '
        ' D.1. Compute the cross-section for [gamma,alpha] in Rh-
103.
        '
        '-----

        for i=0 to (NN - 1)
            sigma(i) = sigma_Rh103(D, best_vector(), energy(i))

```

```

    print #4, energy(i); " , "; sigma(i)
          '(b/atom).
next i

close #4

-----
'
' D.2. Compute the value of lambda(1T).
'
'
'          Eo (MeV)
'          /
' lambda(1T) = | dFLUX/dE(E) * sigma(E) dE
'          /
'          E=0 (MeV)
'
-----

for i=0 to (NN-1)
    ff(i) = sigma(i) * dFLUXdE(i) / barns_per_cm2
next i

' C.1 Energy is in units of MeV and ff() = sigma *
dFlux/dE is in
' photon/(MeV*sec).

lambda_1T = integral(NN, energy(), ff())
lambda_2 = log(2)/t_half-life_Tc99m
lambda_2T = lambda_2

-----
'
' D.3 Calculate the objective function based on the standard
' error between the measured sample radioactivity versus
' the values predicted from the Breit-Wigner
distribution.
'
-----

' D.3.a Compute the radioactivity of the Tc99m based on
the
' absorption cross section.

' D.3.a.1 The original number of Rh-103 atoms is
N(10).

N_10 = m_Rh103 * Avogadro / (A_Rh103/1000) '
(atoms/m^3).

```

```

time, N_2.      ' D.3.a.2 The number of Tc-99m atoms as a function of
* _
N_2 = ((lambda_1T * N_10)/(lambda_1T - lambda_2T))
              (exp(-lambda_2T * t_irradiation) - _
              exp(-lambda_1T * t_irradiation)) * _
              exp(-lambda_2 * t_post_irradiation)

' D.3.a.3 Radioactivity of the Tc-99m inventory.
A_Tc99m = lambda_2 * N_2      ' (Bq).
if A_Tc99m < 0 then A_Tc99m = 0.0

' D.3.a.4 Accumulate the sum of the deviation between
measured and      '
Tc-99m.           '      computed radioactivity of the sample, due to

SE_sum += (A_Tc99m - Measured_Tc99m_Activity(k))^2

print #3, "      Accelerator Energy (MeV):
"; Eo
print #3, "      Activity (Bq)[";k;"]
measured/computed: "; _
                        Measured_Tc99m_Activity(k), A_Tc99m

next k

print #3, "      "
print #3, "      B.2 Standard Error:      "; sqrt(SE_sum)
print #3, "
"
print #3, "      C. Specifics of the Run
"
print #3, "      C.1 Number of generations:      "; generation -
1
print #3, "      C.2 Final 'cost':      ";
cost(index_min_cost)
print #3, "      C.3 Tolerance (based on cost): "; tolerance
print #3, "      C.4 Mean cost:      "; mean_cost
print #3, "      C.5 Standard Error in Cost:      ";
cost_standard_error
print #3, "      C.6 Runtime (s):      "; stop_time -
start_time
print #3, "      C.7 Date:      "; date
print #3, "      C.8 Time:      "; time

close #3

end

```

APPENDIX III

SAMPLE ACTIVATION DATA SHEET

ctm=10
dtm=0
sen=0
coi=0
aui=a003
aui=0
auxsys=0
rtcuse=1
tct=100
tp0=62880
tp1=65535
tp2=65535
dor=f
dac=0
diguse=0
digval=0
rtprena=0
rtpreset=1000.000
autoinc=0
savedata=0
mpafmt=asc
sephead=0
fmt=asc
smoothpts=5
[ADC1]
range=4096
active=0
prena=0
ltpreset=28800.000
roipreset=10000
roimin=1
roimax=4096
caloff=0.000000
calfact=1.000000
calfact2=0
calfact3=0
calunit=keV
caluse=0
roi=416 510

roi=377 553
REPORT-FILE from written 10/04/2011 08:12:49
realtime=300.275
runtime=300.734
livetime=0.000
singlesum=8672
coincsum=0
TOTALSUM=0
ROISUM=0
ROINET=0
cmline1=1A
[ADC2]
range=4096
active=0
prena=0
ltpreset=36000.000
roipreset=10000
roimin=1
roimax=4096
caloff=0.000000
calfact=1.000000
calfact2=0
calfact3=0
calunit=keV
caluse=0
REPORT-FILE from written 10/04/2011 08:12:49
realtime=300.275
runtime=300.734
livetime=0.000
singlesum=8672
coincsum=0
TOTALSUM=0
ROISUM=0
ROINET=0
cmline1=1B
[ADC3]
range=4096
active=0
prena=0
ltpreset=36000.000
roipreset=10000
roimin=1
roimax=4096
caloff=0.000000
calfact=1.000000
calfact2=0

calfact3=0
calunit=keV
caluse=0
REPORT-FILE from written 10/04/2011 08:12:49
realtime=300.275
runtime=300.734
livetime=0.000
singlesum=8672
coincsum=0
TOTALSUM=0
ROISUM=0
ROINET=0
cmline1=1C
[ADC4]
range=4096
active=1
prena=1
ltpreset=300.000
roipreset=10000
roimin=1
roimax=4096
caloff=3.639040
calfact=0.474351
calfact2=-1.44773e-008
calfact3=0
calunit=keV
caluse=3
calch00=3863.32
calvl00=1836.060000
calch01=1885.48
calvl01=898.042000
calch02=1387.10
calvl02=661.657000
calch03=1752.19
calvl03=834.848000
calch04=2679.46
calvl04=1274.530000
calch05=1069.66
calvl05=511.000000
calch06=177.95
calvl06=88.040000
calch07=742.89
calvl07=356.017000
calch08=163.12
calvl08=80.997100
calch09=280.07

calvl09=136.474000
calch10=249.68
calvl10=122.061000
calch11=2801.87
calvl11=1332.500000
calch12=2466.16
calvl12=1173.240000
calch13=117.83
calvl13=59.541200
REPORT-FILE from 10/04/2011
realtime=300.275
runtime=300.734
livetime=300.000
singlesum=8672
coincsum=0
TOTALSUM=8672
ROISUM=8672
ROINET=8672
cmlne0=10/04/2011 08:07:15
cmlne1=1D
[DATA3,4096]
0
0
0
5
35
38
24
18
35
27
20
23
22
30
31
19
28
26
21
17
18
17
20
14
17

APPENDIX IV

NOMENCLATURE

Alphanumeric

A	Activity (Bq)
barn	1E-24 cm ²
Bq	Becquerel (disintegrations per second)
CBA	Cost-Benefit Analysis
Ci	Curie (3.7E+10 Bq)
DE	Differential Evolution
erg	1E-7 Joules
eV	electron volt
FDG	Flourodeoxyglucose
Gy	gray (100 Rad)
HPGe	High Purity Germanium
IAC	Idaho Accelerator Center
keV	1E+3 eV
LINAC	LINear ACcelerator
mCi	millicurie (1E-3 Curie)
mb	1E-3 barn
MeV	1E+6 eV
PET	Positron Emission Tomography
rad	Radiation Absorbed Dose (100 ergs in 1 gram)
ROI	Return on Investment
RTG	Radioisotope Thermoelectric Generator
SPECT	Single Photon Emission Computed Tomography
uCi	microcurie (1E-6 Curie)

Greek Characters

α	Alpha Particle (helium nucleus)
β^-	Beta Particle (electron)
β^+	Positron (positively charged electron)
γ	Gamma Ray (photon originating from the nucleus)

BIBLIOGRAPHY

Attix, F., Introduction to Radiological Physics and Radiation Dosimetry, John Wiley and Sons. 1986.

Briesmeister, J.F., MCNPTM – A General Monte Carlo N-Particle Transport Code, Version 4C. March 2000

Kahn, Laura H., “The potential dangers in medical isotope production,” Bulletin of the Atomic Scientists, 16 March 2008.

Krane, K., Introductory Nuclear Physics, Massachusetts, John Wiley and Sons. 1988

Lamarsh, J.R., Introduction to Nuclear Engineering, 2nd edition. New York: Addison-Wesley. 1983.

Liberman, M.A., De Groot, J.S., Toor, A., Spielman, R.B., Physics of High-Density Z-Pinch Plasmas, New York: Springer-Verlag. 1999.

Newman, M.E.J., and Barkema, G.T, Monte Carlo Methods in Statistical Physics, Oxford: Clarendon Press. 1999.

Pelowitz, D.B., MCNPXTM User’s Manual, Version 2.5.0. April 2005.

Van der Keur, Henk, “Medical Radioisotopes Production Without a Nuclear Reactor,” Laka Foundation Report, 22 May 2010.

VITA

Daniel Robert Lowe

1246 Silver Knoll Ave.
Las Vegas, NV 89123
(702) 480-5759
lowe@nrcc.unlv.edu

Education

Aug. 2000 to July 2005
B.S.E. Mechanical Engineering (3.66 GPA)
University of Nevada Las Vegas

August 2005 to July 2006
M.S.E. Nuclear Engineering (3.72 GPA)
University of Nevada Las Vegas

Expected in Spring 2012
Ph.D. Nuclear Engineering
Thesis Title: "Novel Production Techniques of Radioisotopes Using Electron Accelerators"
University of Nevada Las Vegas

Technical Experience

National Science Foundation/Research Experience for Undergraduates recipient (Summer 2000)

- Designed a liquid nitrogen powered truck

Research Assistant/Engineer (Fall 2000 to current)

- MCNPX code validated for the Advanced Accelerator Applications initiative. Research included flux predictions, foil irradiations, and shielding design in a Pb/Bi target at the LANSCE facility in Los Alamos.
- Radiation shielding concepts for space habitats. Modeling of the space source term and unique composite materials were analyzed.
- Modeling and shielding concepts for Dense Plasma Focus devices at the Nevada Test Site. MCNPX was used in an iterative process to create the maximum number of neutrons possible per shot.
- Using MCNPX over large Beowulf cluster has been demonstrated. The utilization of 340 computers to solve large MCNPX problems drastically improves performance of the code, especially with input decks that have large geometries and/or very energetic particles. Benchmarking of such systems (network speeds, network packet handling, network latency, CPU speeds, disk speeds) has been studied.

- Used MCNPX to create a fast pulse neutron irradiation assembly for the Nevada Test Site using Dense Plasma Focus devices to drive near critical assemblies (2006-2008)
- Have attended 6 MCNPX classes (2 beginning, 2 intermediate, 1 advanced, 1 short course at ANS meeting) in past 7 years

Part-Time Instructor

- Taught MEG 220 (Pro-Engineer) in the Spring of 2003

Past Projects (funding amount, year of grant, PI or Co-PI, sponsor)

- NSTec Neutron System Design Support Phase 1 (\$9k, 2007, PI, NSTec)
- Varian IntellX Shielding Calculations (\$12k, 2008, PI, Varian SIP)
- NSTec Neutron System Design Support Phase 2 (\$62k, 2008, PI, NSTec)
- Hybridization of an Unmanned Aerial System Platform (\$134k, 2008, Co-PI, AFRL)
- Hybridization of an Unmanned Aerial System Platform (\$163k, 2008, Co-PI, UNLV ARI)
- Active Airflow Control (\$103k, 2008, Co-PI, UNLV UTC)
- Sandia National Lab Shield Calculations Task 47 (\$60k, 2008, Co-PI, Sandia National Lab)
- Neutron Systems Support (\$17k, 2008, Co-PI, NSTec)
- Dense Plasma Focus Support (\$47k, PI, 2009, NSTec)
- Neutron Imaging Calibration Simulations (\$14k, PI, 2009, Remote Sensing Lab Nellis)
- Drag Reduction Proof of Principle (\$56k, PI, 2009, UNLV University Transportation Center and Mendenhall Innovation Program)
- Coaxial Dense Plasma Focus Support (\$29k, PI, 2009, NSTec)
- Neutron Coincidence Modeling Support (\$30k, Co-PI, 2010, Remote Sensing Laboratory Nellis)
- Electromagnetic Pulser Support (\$26k, PI, 2010, NSTec)
- MCNPX Calculations for Neutron Multiplicity (\$23k, Co-PI, 2010, NSTec)
- Simulation of Dense Plasma Focus System to Locate SNM (\$60k, Co-PI, 2010, Remote Sensing Laboratory Nellis)

Awards

- National Science Foundation Research Experience for Undergraduate Recipient (2000)
- Outstanding Presentation in Computational/Mathematical Modeling, ANS Student Conference, Wisconsin (2004)
- Harold and Mayme Stocker Scholarship (2004 to present)
- Mechanical Engineering Outstanding Graduate Award (2005)
- Harriet and Fred Cox Grand Prize Engineering Design Award (2005)
- Silver State Millennium Scholar (2000-2004)

- Dean's Honor List (2000-present)
- John and Mary Hughes Alumni Scholarship (2004)
- National Academy for Nuclear Training Scholarship (2001-2004)
- University of Nevada Las Vegas License Plate Scholarship (2003)

Interests

My interests outside of school include high speed model rocketry, golf, scuba diving, canyoneering, welding, underwater photography, astrophotography and high dynamic range photography. Within school, most of my free time is spent with finite element and computational fluid dynamic programs to aid in the construction of ASME's Human Powered Vehicle or in support of local FIRST robotic teams.

Extra Curricular Activities

- ASME Student Section Vice President (2001-2004)
- ANS Student Section Vice President (2004-2005)
- ANS Student Section Treasurer (2004)
- ASME Human Powered Vehicle Designer
- ASME Human Powered Vehicle Machinist
- Tau Beta Pi Member (2003-current)
- High school mentor for the FIRST Robotics Competition (2004-present)
- ASME UNLV Student Liaison (2007-current)

Publications

- "MCNPX on Computational Clusters Using PVM and MPI", **Lowe, D.**, Wilcox, T., Culbreth, W., ANS Annual Conference, Pittsburg, 2004
- "Benchmarking MCNPX on Heterogeneous Clusters Using PVM and MPI", **Lowe, D.**, Wilcox, T., Culbreth, W., ANS Student Conference 2004
- "Monte Carlo Verification and Modeling of Lead-Bismuth Spallation Targets" Los Alamos National Laboratory 2002
- "Neutron Leakage from Lead-Bismuth Targets: Report for 20-cm diameter and 40-cm diameter Targets" James, M., et. Al. Los Alamos National Lab 2002
- "Dose Calculations for New Imaging Technologies Used in the Detection of Radiological Weapons of Mass Destruction" O'Brien, R., **Lowe, D.**, Patton, P. Health Physics Society 2007 Annual Meeting
- "Comparison Between Region of Interest Selection Techniques Used in Diffusion Tensor Imaging Applied to the Corpus Callosum" **Lowe, D.**, Mangum, J., Patton, P. Health Physics Society 2007 Annual Meeting
- "Investigation of the Reproducibility of Functional Magnetic Resonance Imaging and Diffusion Tensor Imaging" Mangum, J., **Lowe, D.**, Patton, P. Health Physics Society 2007 Annual Meeting

- “Fast Pulse Assembly Design for Neutron Multiplication on a DPF Accelerator” Hagen, E., **Lowe, D.**, O’Brien, R., Pigg, J., 2008 IEEE NSS-MIC Conference, Germany
- “Image Analysis of a Dual Energy Mega-Voltage Cargo Imager Utilizing MCNPX”, O’Brien, R., **Lowe, D.**, Meehan, B., Patton, P., Wilcox, T., 2010 RPSD Topical Meeting, Las Vegas, Nevada
- “The Effects of PMT Voltage on Pulse Shape Discrimination Techniques”, **Lowe, D.**, Meehan, B., 2010 RPSD Topical Meeting, Las Vegas, Nevada
- “Investigating the Effects of PMT Characteristics on Pulse Shape Discrimination Techniques”, **Lowe, D.**, Meehan, B., 2010 RPSD Topical Meeting, Las Vegas, Nevada
- “Evidence of Deuterium-Tritium Fusion in a Deuterium Z-Pinch”, Meehan, B., **Lowe, D.**, O’Brien, R., Molnar, S., Hagen, C., 2010 RPSD Topical Meeting, Las Vegas, Nevada
- “Dense-Plasma Focus for Neutron Resonance Spectroscopy”, O’Brien, R., **Lowe, D.**, Hagen, C., Meehan, B., Molnar, S., 2010 RPSD Topical Meeting, Las Vegas, Nevada